

## SCUBA Mapping of Spitzer c2d Small Clouds and Cores

Chadwick H. Young

*Department of Physical Sciences, Nicholls State University, Thibodaux, Louisiana 70301*

Tyler L. Bourke

*Harvard-Smithsonian Center for Astrophysics, Cambridge, MA 02138, USA*

Kaisa E. Young

*Department of Physical Sciences, Nicholls State University, Thibodaux, Louisiana 70301*

Neal J. Evans II

*Department of Astronomy, The University of Texas at Austin, Austin, Texas 78712–1083*

Jes K. Jørgensen

*Harvard-Smithsonian Center for Astrophysics, Cambridge, MA 02138, USA*

Yancy L. Shirley

*Steward Observatory, University of Arizona, Tucson, AZ 85721*

Ewine F. van Dishoeck

*Leiden Observatory, P.O. Box 9513, 2300 RA Leiden, Netherlands*

Michiel Hogerheijde

*Leiden Observatory, P.O. Box 9513, 2300 RA Leiden, Netherlands*

### ABSTRACT

We present submillimeter observations of dark clouds that are part of the Spitzer Legacy Program, From Molecular Cores to Planet-Forming Disks (c2d). We used the Submillimetre Common User’s Bolometer Array to map the regions observed by Spitzer by the c2d program to create a census of dense molecular cores including data from the infrared to the submillimeter. In this paper, we

present the basic data from these observations: maps, fluxes, and source attributes. We also show data for an object just outside the Perseus cloud that was serendipitously observed in our program. We propose that this object is a newly discovered, evolved protostar. Finally, these data are publicly available at <http://peggysue.as.utexas.edu/SIRTF/DATA/>.

*Subject headings:* stars: formation, low-mass

## 1. Introduction

In recent years, significant progress has been made toward a theory for the formation of low mass stars, which are the likely sites for the formation of planetary systems. Maps of submillimeter dust continuum emission are excellent tracers of the column density and mass. Dust continuum emission has been used to map both large clouds (e.g. Motte, André, & Neri 1998; Johnstone, Di Francesco, & Kirk 2004; Enoch et al. 2006) and smaller cores (e.g., Shirley et al. 2000; Visser et al. 2002; Young et al. 2003; Kirk et al. 2005).

Studies of small cores provide complementary advantages to less-biased surveys of large clouds. By focusing on regions already known to have dense gas, we can study their properties in more detail. The large scale surveys can in turn check the biases that are introduced. This paper presents data on dust continuum emission toward a large number of small cores.

For a full analysis, data at submillimeter wavelengths should be combined with data through the infrared. The Spitzer Legacy program, From Molecular Cores to Planet-Forming Disks (c2d), described by Evans et al. (2003) has obtained extremely sensitive observations from 3.6 to 70  $\mu\text{m}$  toward 105 small cores (Huard et al. 2006). In order to obtain the full benefit of this database, it is crucial to add data at longer wavelengths where the dust emission is optically thin.

We have mapped 38 small cores, which were initially included in the c2d program, using the Submillimetre Common-User Bolometer Array (SCUBA) at both 850 and 450  $\mu\text{m}$ . Because of time constraints, 15 of these cores were dropped from the c2d program, though some were covered by the large cloud map of Perseus (Jørgensen et al. 2006, Rebull et al. 2006). Together with other complementary data at optical and near-infrared wavelengths, our observations provide a comprehensive catalog of multi-wavelength data for a sample of small molecular cores. The goal of this paper is to present the SCUBA data in a uniform way, consistent with other papers presenting submillimeter continuum data on the c2d cores and clouds. We leave detailed analysis to later papers that combine these data with the c2d data.

## 2. Observations and Data Reduction

### 2.1. Sample

The sample was drawn from those cores originally included in the c2d observation plan. In turn, those cores had been drawn from catalogs of nearby cores that have molecular line maps (Lee & Myers 1999; Jijina et al. 1999; Lee et al. 2001). The gas in these cores is well-studied, mostly by mapping observations of the 1.3 cm line of  $\text{NH}_3$  (Benson & Myers 1989) and the 3 mm line of  $\text{N}_2\text{H}^+$  (Caselli et al. 2002). These cores are all relatively nearby, within 450 pc, so their maps have good spatial resolution. A few cores have been observed in the submillimeter before, but not over a region as large as that mapped by the Spitzer Space Telescope. In these observations, we have matched the SCUBA maps to cover the same area as the Spitzer maps; in most cases, these maps are  $5' \times 5'$ , but they are sometimes larger.

Table 1 lists the central right ascension and declination for each region observed with SCUBA. This table also has the core’s associated cloud, if relevant, and the distance, using the standard distances adopted for the c2d project (Huard et al. 2006). We note whether submillimeter emission was detected in our observations (Y or N). For those with a submillimeter detection, we list whether the submillimeter core has an IRAS detection (within  $1'$  of the submillimeter peak); these IRAS sources were chosen based on the criteria given by Lee & Myers (1999). We also list whether there was an IRAS source in those maps with no detected submillimeter emission. For maps with more than one clearly separated source, we give multiple entries in the IRAS and SCUBA columns (e.g., YNY). Next, we indicate whether the core was observed in the cores part of the c2d program (Y) or covered by the Perseus cloud map (P); the names for these objects are listed in boldface type. Table 1 includes the  $3\text{-}\sigma$  limit for each map at both 850 and 450  $\mu\text{m}$ , followed by the atmospheric opacity during the observations, again at both wavelengths. Because the goal of this project was to cover the same observed area as in the c2d program, we often observed in weather conditions that were inadequate for good 450  $\mu\text{m}$  maps. This allowed us to create large maps, but the quality of the 450  $\mu\text{m}$  data, as a result, is not sufficient to analyze dust temperature, emissivity, etc.

We had intended to observe Per9, whose position is in Caselli et al. (2002). However, we improperly entered the coordinates at the telescope and mistakenly observed a field that happens to be centered on 2MASS 0347392+311912. This field is about  $30''$  from the edge of the c2d coverage for the Perseus cloud. We discuss the nature of this object in Section 4.

## 2.2. Observations

We observed these cores with the 15 m James Clerk Maxwell Telescope (JCMT) beginning in January 2002 and ending February 2004. We were granted time during each semester between these dates. However, the data collected during the semester 02A and December 2002 to February 2003 were not usable because of technical problems with the JCMT. These are the program identification designations for our observations: M/01B/N13, M/02A/N18, M/02B/N04, M/03A/N08, and M/03B/N10.

We used the scan mapping technique (Holland et al. 1999), which is used to map regions much larger than SCUBA’s field of view. Through this method, the telescope scans across the field while chopping by 30, 44, and 68 degrees in the scan direction, which is in both the direction of right ascension and declination. The chopping removes sky variations and DC offsets, and it creates a difference map of the source, a positive and negative source separated by the chop throw, which must be restored by software.

During the course of observations, we measured  $\tau_{850}$  and  $\tau_{450}$  with frequent skydips, compared these data with  $\tau_{CSO}$ , and found good agreement. Finally, we observed several cores for flux calibration: CRL 618, Mars, Uranus, and IRC10216. We generally observed at least 2-3 calibrators during an observing shift.

## 2.3. Data Reduction

We analyzed and reduced our data with the SCUBA User’s Reduction Facility (SURF) (Jenness & Lightfoot 1997); we also closely followed the reduction methods of Pierce-Price (2001). Our reduction entailed flatfielding, extinction correction, removal of bad pixels, removal of baselines, and the coadding and rebinning of the maps.

To correct the data for atmospheric extinction, we measured  $\tau_{850}$  and  $\tau_{450}$  from skydips that were completed at the time of each map; these values for  $\tau$  are listed in Table 1 and Table 2 for the cores and calibrators, respectively.

For the removal of bad pixels, we first used SURF’s “despike2” tool, which removes spikes from scanmap observations. This package has 2 criteria for despiking. The first considers each data point and asks how disparate it is from the two adjacent data points. If this difference is greater than a certain number of standard deviations for the scan (NSIGMA), the data point is rejected. We use NSIGMA=4. The second criterion convolves the data with a three sample box and uses NSIGMA in the same way. In addition, we have used “sclean” to interactively search all of the data for bad pixels.

We use SURF’s “scan\_rlb” to remove the baselines from the extinction corrected and cleaned data. We assume there is no emission at the end of each scan, which is generally true, and use the linear method of baseline removal. In this way, scan\_rlb fits the baseline to the end of each scan and then applies it to the remaining scan.

Next, we rebin the data, with baselines removed, to create the dual-beam map. We used pixels appropriate for Nyquist sampling (3.5” and 7.5” for 450 and 850  $\mu\text{m}$ , respectively) and do not smooth the maps; smoothing of the maps often causes artifacts from the data reduction to appear as real emission (greater than  $3-\sigma$ ). At this point, we examine each rebinned, dual-beam map to search for evidence of bad data, such as stripes or other artifacts, missed during the despiking and cleaning tasks.

The rebinned maps are the telescope’s dual-beam function convolved with the sky. We use “remdbm” to remove the dual-beam signature from the map. This package uses the Emerson2 (Emerson 1995; Emerson et al. 1979) technique to deconvolve the data and create the single-beam map of the source. We use no high-frequency filtering. We assess the RMS noise of the map with Starlink’s “stats” package and create the maps in Figure 1. The contours begin at  $2-\sigma$  and increase by  $2-\sigma$ ; greyscale begins at  $-2-\sigma$  and increases to the image maximum. Crosses mark the position of IRAS sources, which were selected using the criteria of Lee & Myers (1999).

We have used Starlink’s Extractor, which is based on SExtractor (Bertin 2003), to extract source information for each of the maps in Figure 1 (Chipperfield & Draper 2004). This includes the source positions (barycenter), semi-major and semi-minor axes, and aspect ratios in Table 3. The aspect ratio is the ratio of major to minor axes as measured at the  $3-\sigma$  threshold limit except for L1251C; where we used a threshold limit of  $5-\sigma$ . The  $3-\sigma$  limit, for L1251C, extracted a source that was much larger than the obviously compact and embedded core. In Figure 1, we have overlaid, on the maps, an ellipse that matches the extracted source by Extractor. For those observations with especially large fields, maps covering just the central regions are shown in Figure 2.

## 2.4. Calibration

In Table 2, we list flux conversion factors (FCF) for all calibrators observed during the course of this project. To calculate the FCF, we divide the flux of the calibrator, which is assumed to be a point source, by the total data counts (i.e. volts) in a given aperture. To determine the FCF for a 20” aperture, for example, we divide the flux of the calibrator by the total data counts for a 20” aperture, which gives the FCF in units of Jy/Volt. Then, we

use this FCF to convert the data counts for the cores into flux units (for a 20'' aperture). This method of calibration has been used by a number of authors (Shirley et al. 2000; Young et al. 2003, e.g.) and is superior to using beam-sized apertures because of the significant and variable sidelobes on the JCMT's beam at 850 and 450  $\mu\text{m}$ . These sidelobes, at 850  $\mu\text{m}$ , can extend to 50'' even though the beam size is  $\sim 15''$  (Shirley et al. 2000).

In utilization of the FCF, we simply average all values, except those for Jupiter and IRC 10216, and give this average and standard deviation in Table 2. As suggested on the SCUBA webpage, we do not use Jupiter and IRC10216 for flux calibration. (<http://www.jach.hawaii.edu/JCMT/con>) We do not use FCFs when the uncertainty approaches 100%, as for the 450  $\mu\text{m}$  FCFs for 80'' and 120'' apertures, but we list them in Table 2 along with all of the average calibration factors.

In Table 2, we also give the FWHM of a Gaussian fit to the JCMT beam pattern at 850  $\mu\text{m}$ . We fit a Gaussian to the observed intensity profile with Starlink's `psf` routine (setting `gauss=True`) and deconvolve the measured beam size for the planet diameter (Uranus and Mars have semi-diameters of 1''.72 and 3''.67, respectively). The average FWHM of the beam, over all nights, was  $15''.5 \pm 0''.5$ . The nominal beam at 450  $\mu\text{m}$  is about 8'', but it can be as large as 11'' (Young et al. 2003). Because the quality of the 450  $\mu\text{m}$  data is poor, we do not calculate the 450  $\mu\text{m}$  beam profile for these observations.

We have calculated fluxes for each source whose size and shape were determined by Extractor. To determine the FCF for these non-circular apertures, we have fit a function to the FCFs of the circular apertures. Because the sidelobes contribute significantly to the aperture sums, the FCF decreases as the area of the aperture increases. In Figure 3, we show the average FCFs for the 20'', 40'', 80'', and 120'' apertures; the solid line in this plot is a fit to these data:  $FCF = 140 \text{Area}^{0.15}$ , where *Area* is the area in square arcseconds of the aperture. For the non-circular apertures, we calculate the area ( $\pi ab$ ) and determine the FCF from the above relationship. Then, we calculate the flux and ascribe a 30% uncertainty to this measurement, which is a liberal estimate of the flux uncertainty at 850  $\mu\text{m}$ . The fluxes in the elliptical apertures are in Table 3, and the fluxes in the fixed circular apertures of different diameters are given in Table 4. The apertures are those agreed to for papers presenting ancillary data to the c2d project. These ancillary continuum data are in preparation for publication and include observations of the c2d cores from Max-Planck-Millimeter-Bolometer (Kreysa et al. 1998, MAMBO), the Submillimeter High Angular Resolution Camera II (Dowell et al. 2003, SHARCII), and the Sest Imaging Bolometer Array (Nyman et al. 2001, SIMBA). In Figure 4, we show the MAMBO data as greyscale with the SCUBA 850  $\mu\text{m}$  observations represented by contours, as in Figure 1. There is good agreement between these sets of data in representing the detected continuum emission.

Kirk et al. (2005) observed two of these sources with SCUBA; for L1521F, they measured the fluxes in a  $150''$  aperture:  $3.23 \pm 0.23$  Jy at  $850 \mu\text{m}$  and  $12.4 \pm 2.4$  Jy at  $450 \mu\text{m}$ . These are compared to our measurements of  $4.2 \pm 0.7$  Jy at  $850 \mu\text{m}$  ( $120''$  aperture) and  $13.3 \pm 7.2$  Jy at  $450 \mu\text{m}$  ( $40''$  aperture). For L43, Kirk et al. (2005) measured  $5.4 \pm 0.23$  and  $28.6 \pm 1.8$  Jy (at  $850$  and  $450 \mu\text{m}$ ), which compares to our measured values of  $4.8 \pm 1.2$  and  $15.0 \pm 8.1$  Jy.

### 3. Results

In this section, we give the basic results for these observations: maps, fluxes, and characteristics of the cores. Further analysis of these data will follow in later papers and will include Spitzer observations and other ancillary data (near-infrared, millimeter, etc.).

Of the 38 cores observed with SCUBA, 13 were not detected at either  $850$  or  $450 \mu\text{m}$ . For these cores and the detected objects, we list the  $3\text{-}\sigma$  noise level in Table 1, starting with source PER7A. These cores do not appear in the other tables. The maps for the detected cores are shown in Figure 1. For those observations with especially large fields, maps covering just the central regions are shown in Figure 2. In both of these figures, crosses represent IRAS sources selected by the criteria of Lee & Myers (1999), and the ellipses are the sources chosen by Extractor.

#### 3.1. Size, Shape and Mass

In Table 3, we give the size and aspect ratio of each core as measured at the  $3\text{-}\sigma$  level with Starlink’s Extractor. We also list the  $850 \mu\text{m}$  flux within the aperture described by this size and aspect ratio; the isothermal mass of each core is derived from that  $850 \mu\text{m}$  flux, assuming a temperature of 15 K (Young et al. 2003, see Equation 2); the dust opacity used in these calculations is  $\kappa_\nu = 0.018 \text{ cm}^2\text{g}^{-1}$  (for OH5 dust; Ossenkopf & Henning 1994). The assumed temperature is relevant; a variation from 10 K to 20 K in isothermal temperature causes an increase in the mass by a factor of 3.3. The sizes are, with one exception, much larger than the beam, so deconvolution of the beam is unnecessary. The very compact core is not included in the plots.

In Figure 5, we plot histograms of the isothermal masses, aspect ratios, and core areas as reported in Table 3. The difference in the position of the peak pixel and the barycenter position (i.e., the center of the fitted ellipse) is also shown as a histogram in this figure; this is a measure of axisymmetry. The core area is equal to  $\pi ab$ , the area of an ellipse. In order

to maintain consistency with other c2d ancillary data papers to come, we show the data for only those cores observed in the c2d program (i.e. the boldfaced objects in Table 3). The dotted lines represent the histogram for the entire sample of cores.

In Figure 6, we plot the core mass against the size and aspect ratio of the cores (as measured at the  $3\text{-}\sigma$  level); the data for those cores observed in the c2d program are represented by filled triangles; the cores not observed by c2d are shown as open triangles. The lines in the left panel (with area) represent what is expected for this relationship in cores with constant column density (flat) and constant density ( $M \propto \text{area}^{1.5}$ ).

The dust mass increases with size as one might expect, though the scatter is large. There are also a number of cores that have low masses despite their large core size. Perhaps, these objects are cold, starless cores.

### 3.2. Multiplicity

Several of the maps contain more than one dense core: IRAM 04191+1522, L1082A, L1157, L1221, L1251E, L43, and Per4. Three other objects have some extended emission, which is either real or an artifact of the double-beam deconvolution (Pierce-Price 2001): B35A, CB68, and L1251C. For B35A, at least, the extended emission does appear to be real because the  $\text{N}_2\text{H}^+$  map shows similar structure (Caselli et al. 2002). The  $\text{N}_2\text{H}^+$  map of L1251C is also similar to the  $850\ \mu\text{m}$  continuum image. CB68 was mapped by Huard et al. (1999), and their map, while much smaller and more sensitive than ours, does not appear to show the extended emission in Figure 1.

In all but one case, only one object in each of the multiple core systems was detected by IRAS. This implies that either these multiple cores are at different stages of evolution or that some of the cores are forming objects with lower masses than their companion and hence are not detected by IRAS. With the Spitzer Space Telescope, we have begun to unravel the mystery of these cores. For example, IRAM 04191+1522 does harbor an infrared source detected with IRAC and MIPS (Dunham et al. 2006), but L43-SMM does not appear to harbor an embedded source down to very low luminosities (Huard et al. 2006).

## 4. 2MASS 0347392+311912

We inadvertently observed 2MASS 0347392+311912, having intended to observe a known core in Perseus instead. The source lies outside of the c2d observations for Perseus, so we have no mid- or far-infrared data. The 2MASS source, however, did have detectable



submillimeter emission at  $850\ \mu\text{m}$  (0.2 Jy).

In Figure 7, we show the  $850\ \mu\text{m}$  data overlaid on 2MASS K-band and DSS R-band images. In both the near-infrared and optical maps, the source appears pointlike and is clearly detected. In Figure 8, we plot the SED for this source, including the near-infrared data from 2MASS and B, R, and I measurements from the USNO B1.0 catalog. The SED peaks at  $1.65\ \mu\text{m}$  (H), but has substantial submillimeter emission (0.1 Jy at  $850\ \mu\text{m}$ ). This source may be a previously unknown protostar, which is possibly near the Perseus molecular cloud.

## 5. Summary

We have presented SCUBA observations of low-mass cores that were initially proposed to be observed with the Spitzer Space Telescope as a part of the c2d Legacy Program. We describe these observations and the data reduction and analysis. In addition, we show the maps, source fluxes, and source sizes. The core mass has been calculated from the  $850\ \mu\text{m}$  fluxes, and we analyze how the mass varies with source size and shape. We find several small clouds with multiple, distinct cores, but, for most regions, only one of the cores is detected by IRAS. Finally, we present inadvertent observations of an object near Perseus that may be a newly discovered protostar. All data presented here are publicly available as FITS images at <http://peggysue.as.utexas.edu/SIRTF/DATA/>.

## 6. Acknowledgements

The authors acknowledge the data analysis facilities provided by the Starlink Project which is run by CCLRC on behalf of PPARC. We are also grateful to the JCMT support scientists Remo Tilanus, Vicky Barnard, and Douglas Pierce-Price for much needed help in observing and data reduction. Support for this work, part of the Spitzer Legacy Science Program, was provided by NASA through contract 1224608 issued by the Jet Propulsion Laboratory, California Institute of Technology, under NASA contract 1407. Astrochemistry in Leiden is supported by a NWO Spinoza grant and a NOVA grant. This work was also supported by NASA grants NAG5-10488 and NNG04GG24G.

## REFERENCES

Benson, P.J. & Myers, P.C., 1989, ApJS, 71, 89

- Bertin, E., SExtractor v2.3 User's Manual (Paris: Institut d'Astrophysique)
- Caselli, P., Benson, P.J., Myers, P.C., & Tafalla, M., 2002, *ApJ*, 572, 238
- Chipperfield, A.J. & Draper P.W., 2004, *Starlink User Note* 226.8
- Dobashi, K., Bernard, J.-P., Yonekura, Y., & Fukui, Y., 1994, *ApJS*, 95, 419
- Dowell, C.D., et al., 2003, *Proc. SPIE*, 4855, 73
- Dunham, M.M., et al., 2006, submitted, *ApJ*
- Elias, J.H., 1978, *ApJ*, 224, 857
- Emerson, D. T. 1995, in *ASP Conf. Ser. 75, Multi-feed Systems for Radio Telescopes*, ed. D. T. Emerson & J. M. Payne (San Francisco: ASP)
- Emerson, D. T., Klein, U., & C.G.T. Haslam, 1979, *A&A*, 76, 92
- Enoch, M. L., et al. 2006, *ApJ*, 638, 293
- Evans, N.J. II, et al., 2003, *PASP*, 115, 965
- de Geus, E.J., de Zeeuw, P.T., & Lub, J., 1989, *A&A*, 216, 44
- Goldsmith, P.F., Snell, R.L., Hemeon-Heyer, M., & Langer, W.D., 1984, *ApJ*, 286, 599
- Holland, W.S., et al., 1999, *MNRAS*, 303, 659
- Huard, T.L., Sandell, G., & Weintraub, D.A., 1999, *ApJ*, 526, 833
- Huard, T.L., et al., 2006, in prep.
- Jenness, T. & Lightfoot, SURF, SCUBA User Reduction Facility ver. 1.5-1 User's Manual (Hilo: Joint Astronomy Centre)
- Jijina, J., Myers, P.C., & Adams, F.C., 1999, *ApJS*, 125, 161
- Jørgensen, J. K. et al. 2006, *ApJ*, in press
- Johnstone, D., Di Francesco, J., & Kirk, H. 2004, *ApJ*, 611, L45
- Kauffmann, J., 2006, in prep.
- Kirk, J.M., Ward-Thompson, D., & André, P. 2005, *MNRAS*, 360, 1506
- Kreysa, E., et al., 1998, *Proc. SPIE*, 3357, 319

- Kun, M., 1998, *ApJS*, 115, 59
- Kun, M. & Prusti, T., 1993, *A&A*, 272, 235
- Lee, C.W. & Myers, P.C., 1999, *ApJS*, 123, 233
- Lee, C.W., Myers, P.C., & Tafalla, 2001, *ApJS*, 136, 703
- Motte, F., André, P., & Neri, R. 1998, *A&A*, 336, 150
- Murdin, P. & Penston, M.V., 1977, *MNRAS*, 181, 657
- Nyman, L., et al., 2001, *The Messenger*, 106, 40
- Ogura, K. & Sugitani, K., 1998, *PASA*, 15, 91
- Ossenkopf, V. & Henning, T., 1994, *A&A*, 291, 943
- Pierce-Price, D.P.I., 2001, Ph.D. dissertation
- Rebull, L., et al., 2006, in prep.
- Shirley, Y. L., Evans, N. J., II, Rawlings, J. M. C., & Gregersen, E.M., 2000, *ApJS*, 131, 249
- Straizys, V., Cernis, K., & Bartasiute, S., 2003, *A&A*, 405, 585
- Straizys, V., Cernis, K., Kazlauskas, A., & Meistas, E., 1992, *Baltic Astron.*, 1, 149
- Visser, A. E., Richer, J. S., & Chandler, C. J. 2002, *AJ*, 124, 2756
- Woermann, B., Gaylard, M. J., & Otrupcek, R. 2001, *MNRAS*, 325, 1213
- Yonekura, Y., Dobashi, K., Mizuno, A., Ogawa, H., & Fukui, Y., 1997, *ApJS*, 110, 21
- Young, C.H., Shirley, Y.L., Evans, N.J., II, & Rawlings, J.M.C., 2003, *ApJS*, 145, 111

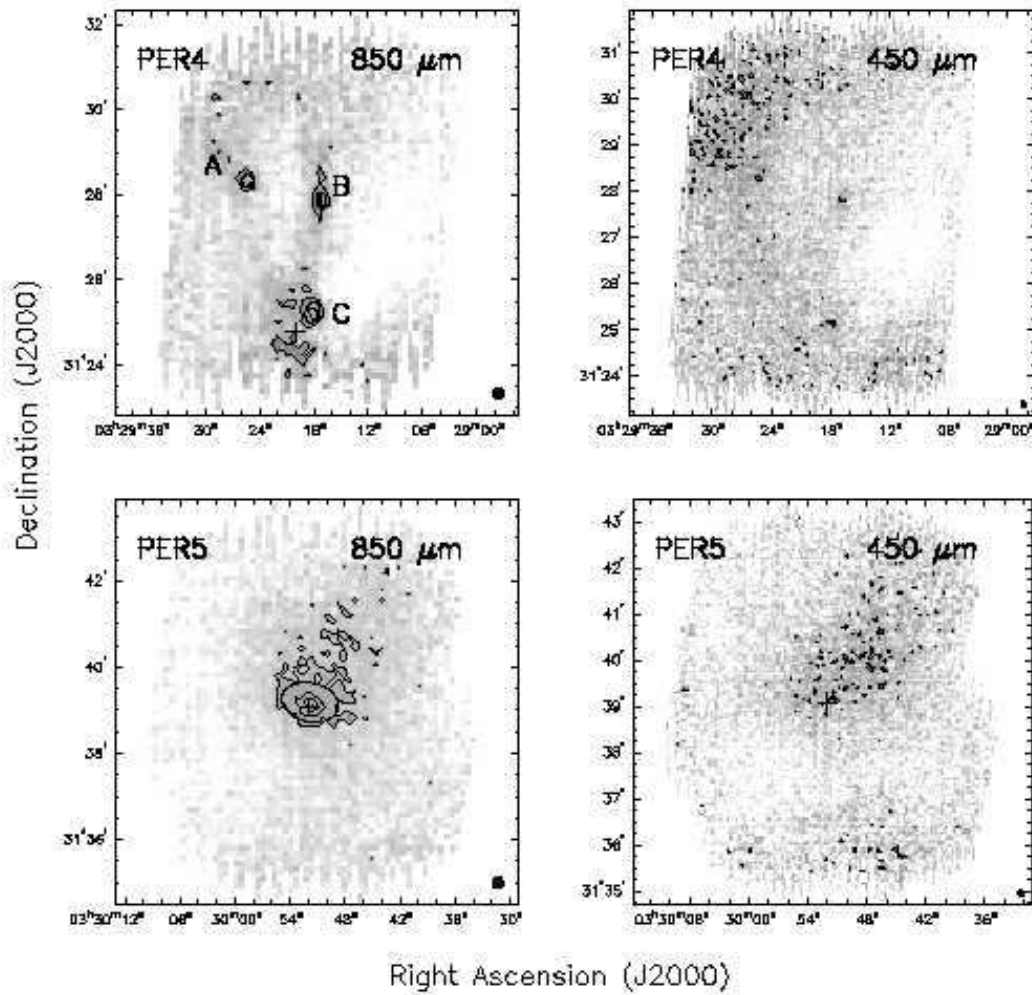


Fig. 1.— We show the 850 and 450  $\mu\text{m}$  maps for the cores in Table 1. Contours begin at  $2\text{-}\sigma$  and increase by  $2\text{-}\sigma$ ; greyscale begins at  $-2\text{-}\sigma$  and increases to the image maximum. Crosses mark the position of IRAS sources in the field. The ellipses show the size and shape of the

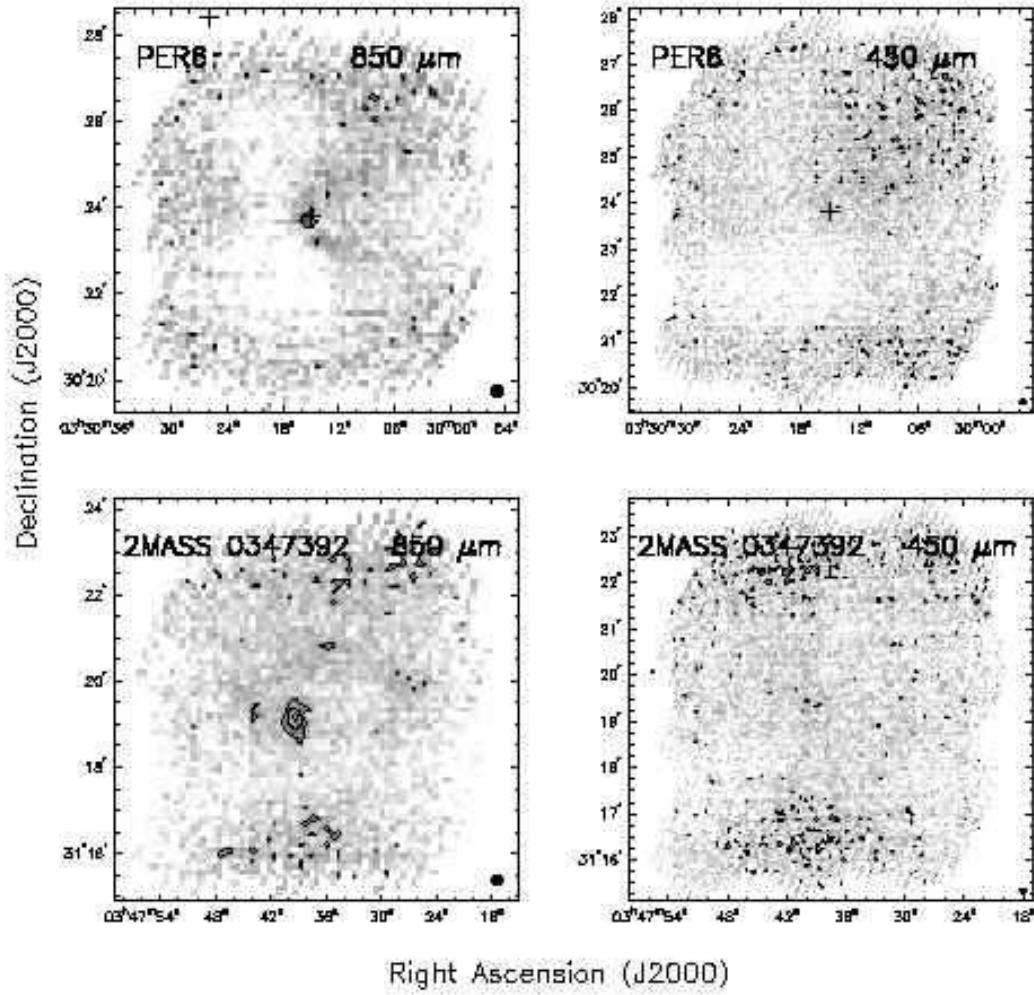


Fig. 1.— continued...

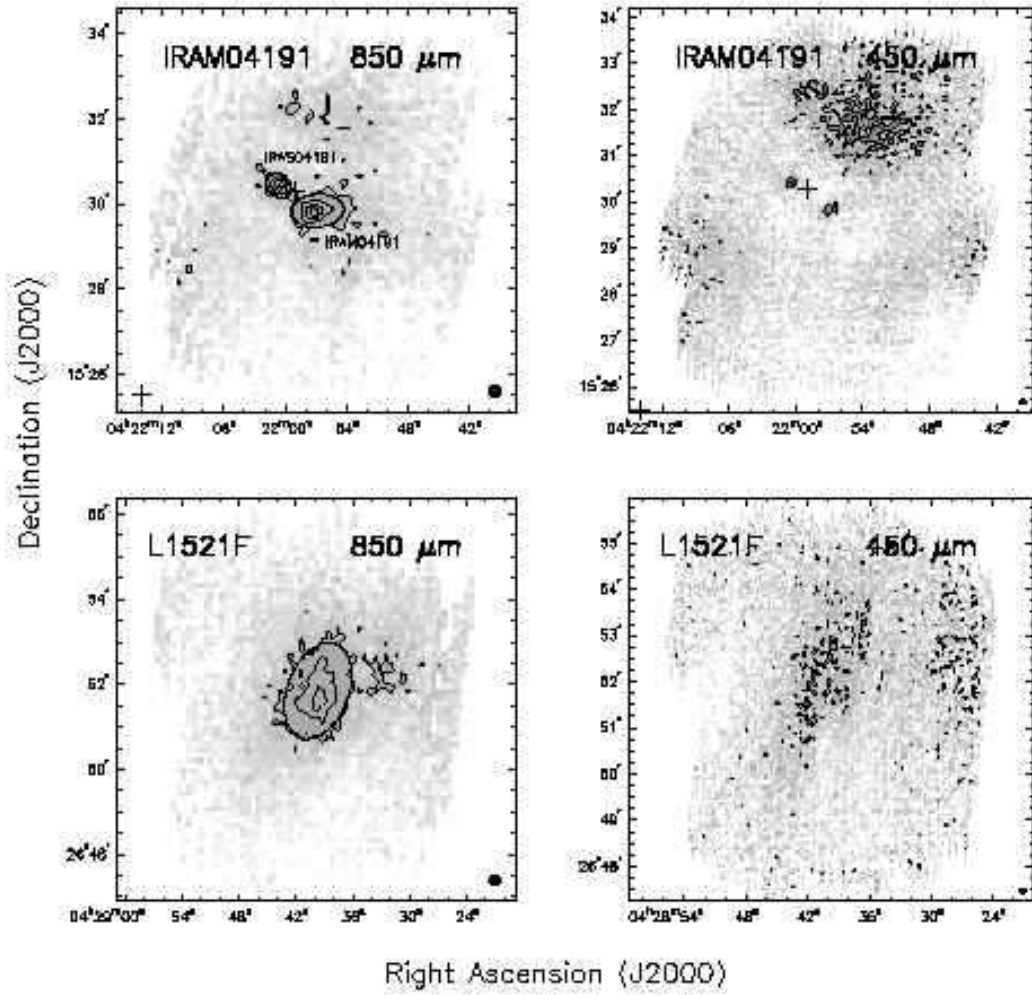


Fig. 1.— continued...

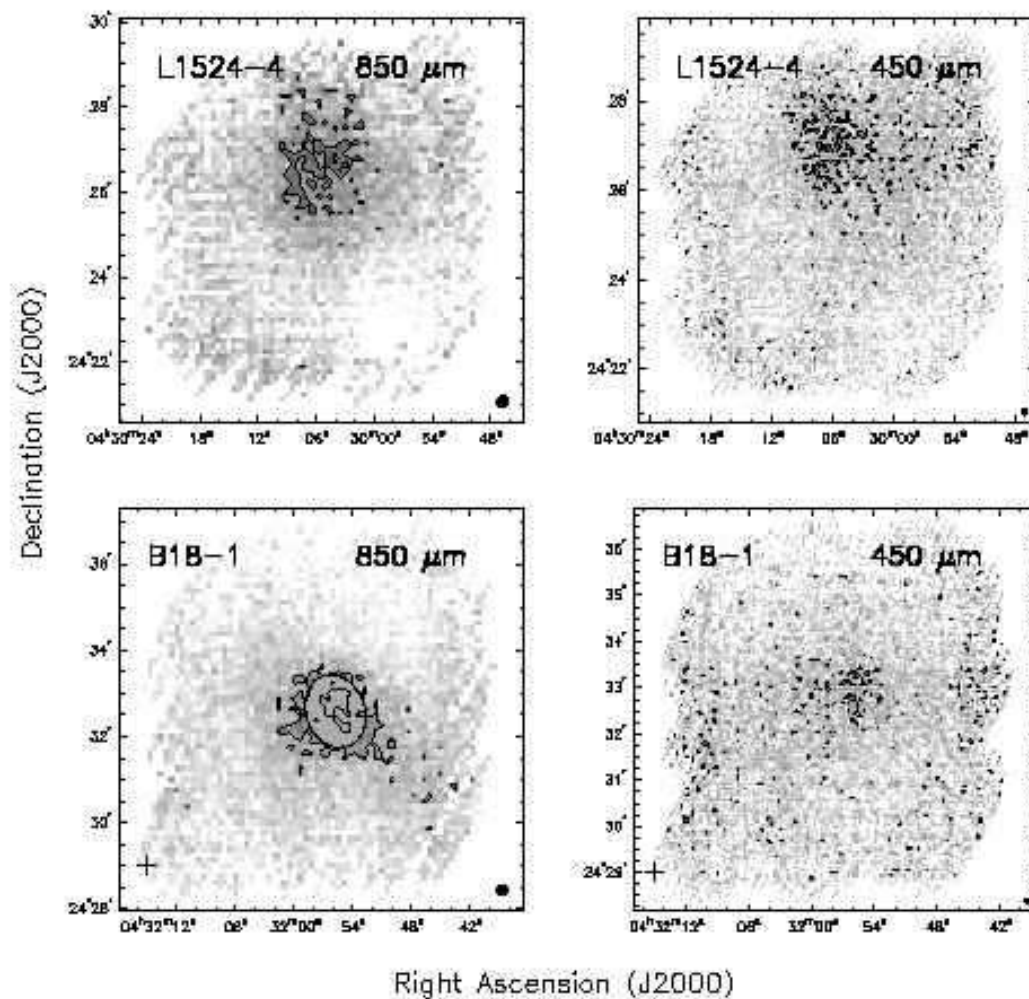


Fig. 1.— continued...

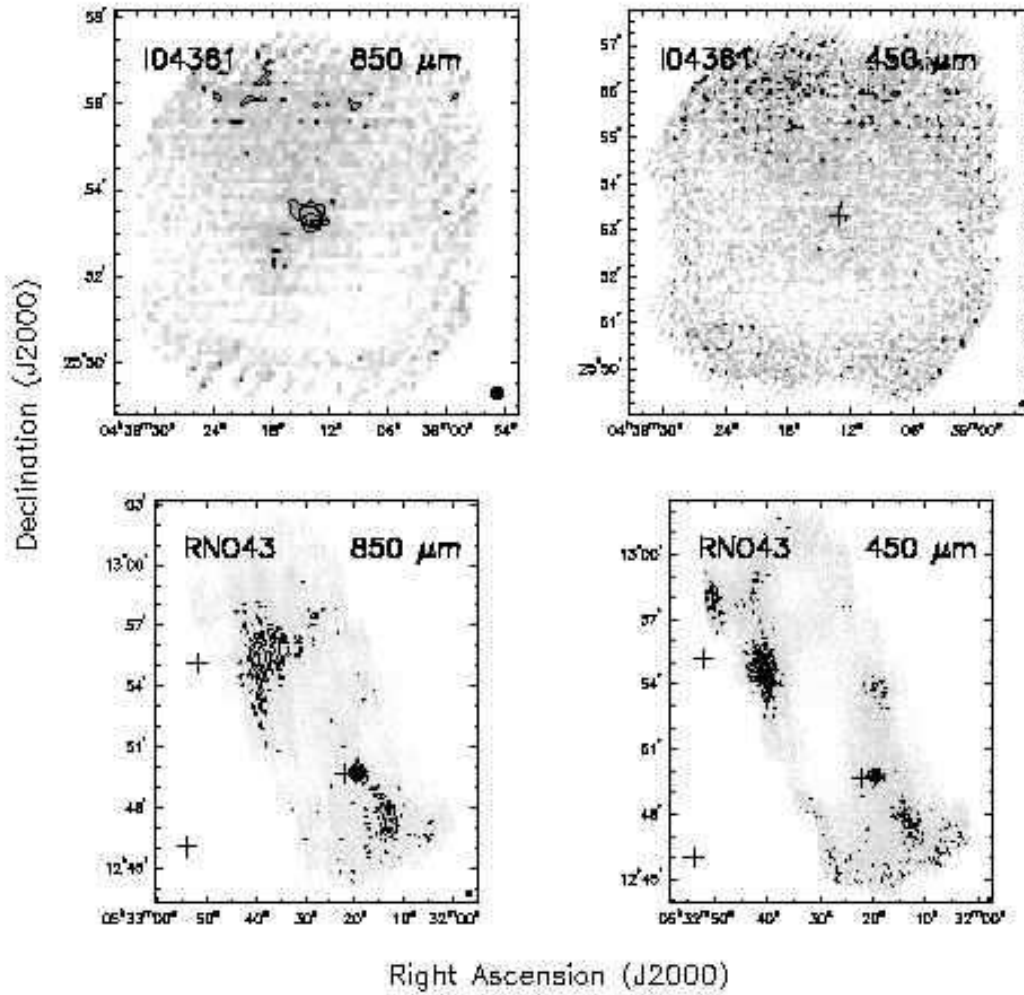


Fig. 1.— continued...



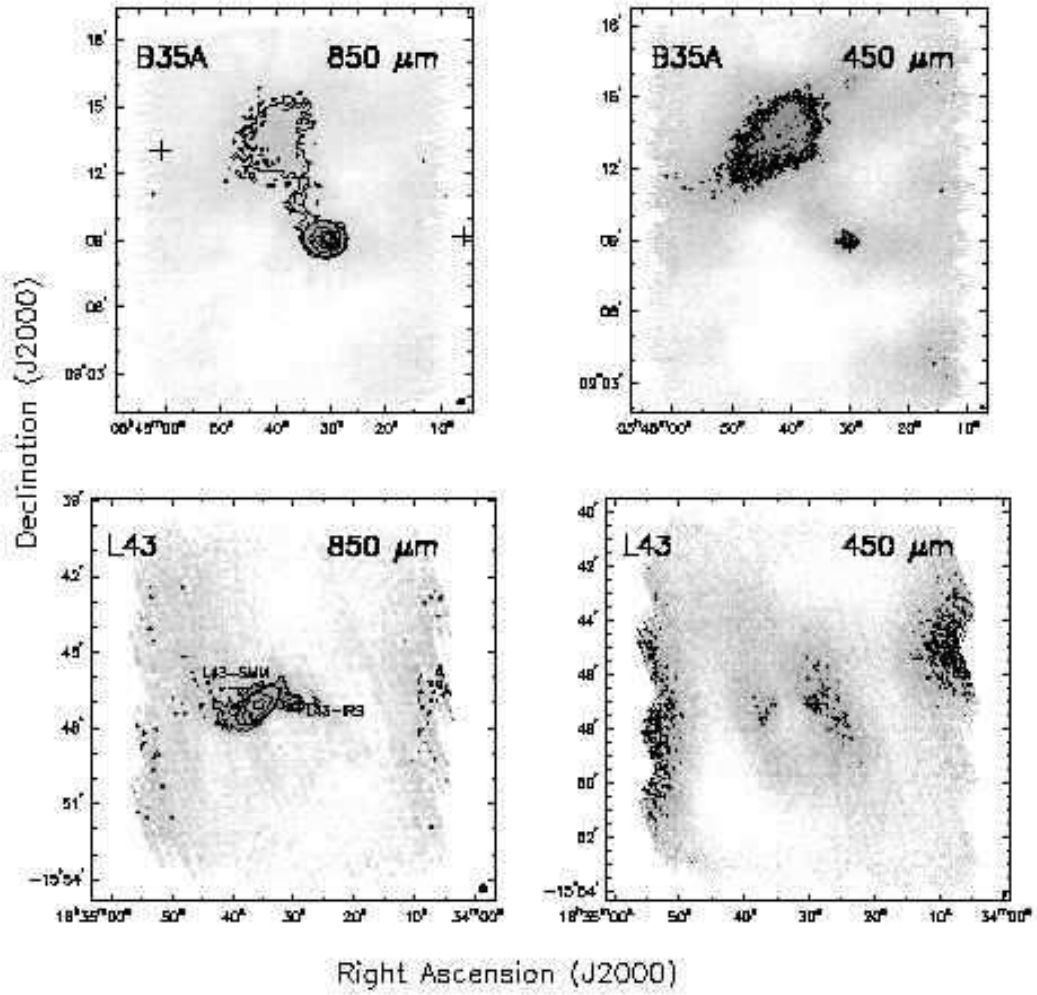


Fig. 1.— continued...

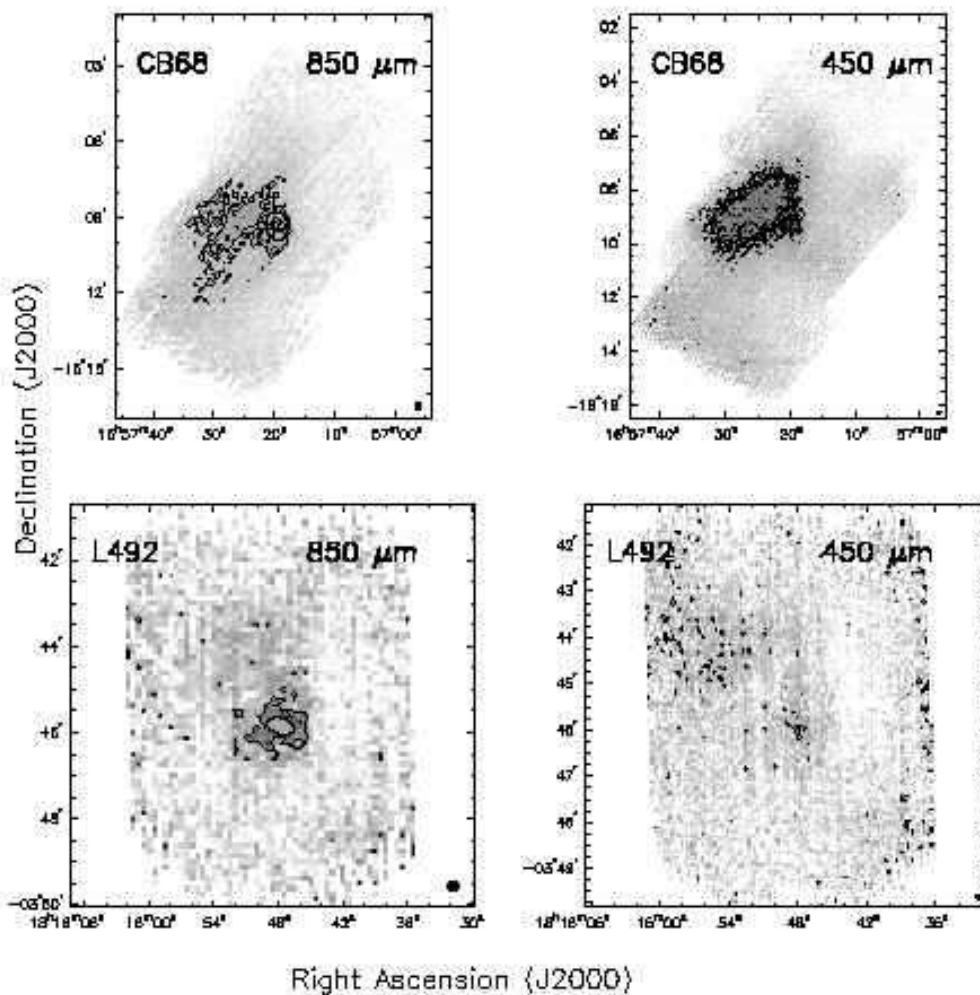


Fig. 1.— continued...

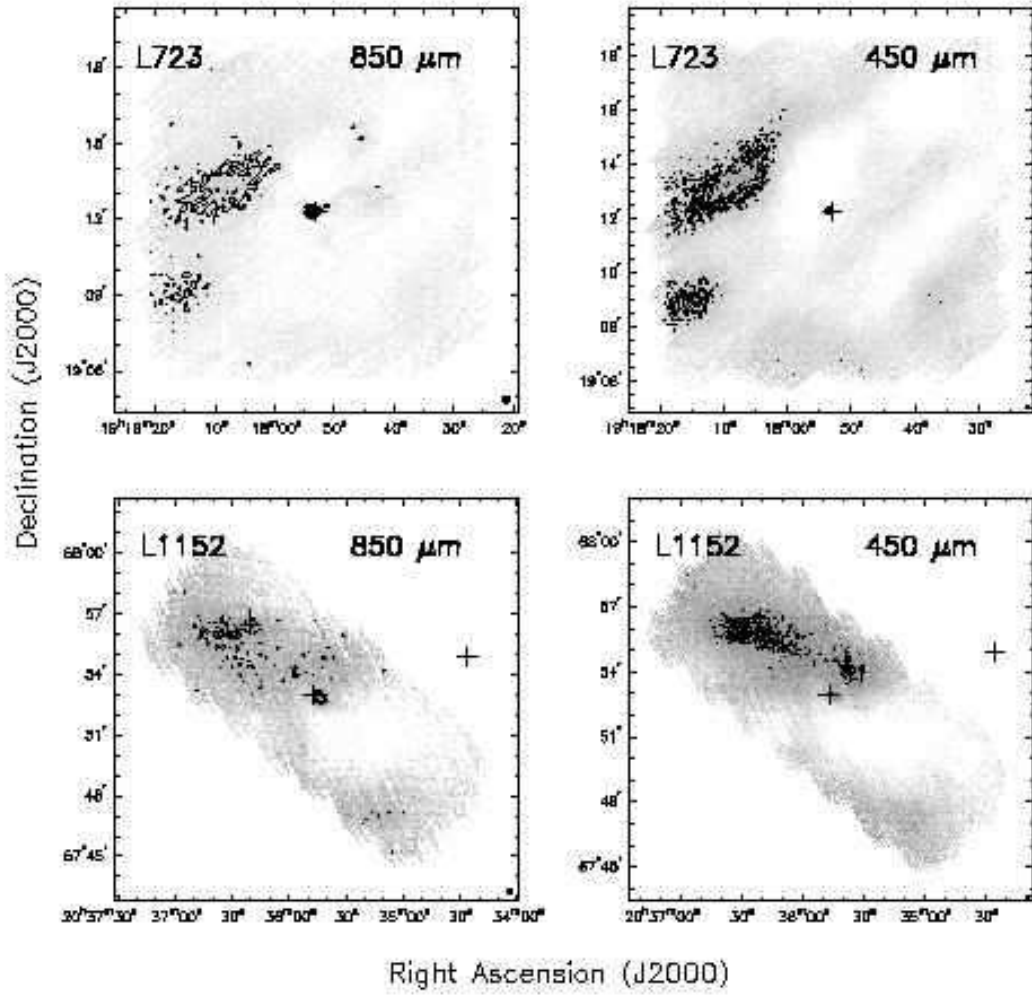


Fig. 1.— continued...

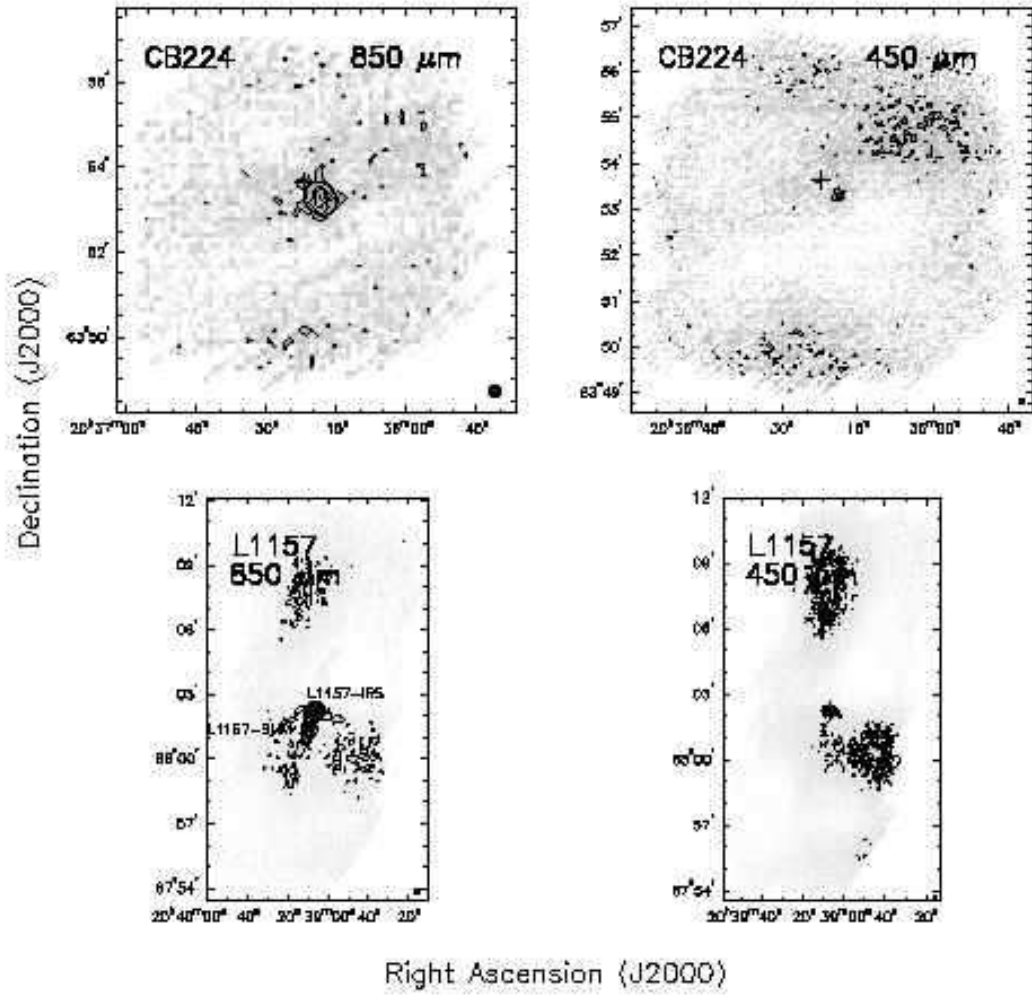


Fig. 1.— continued...

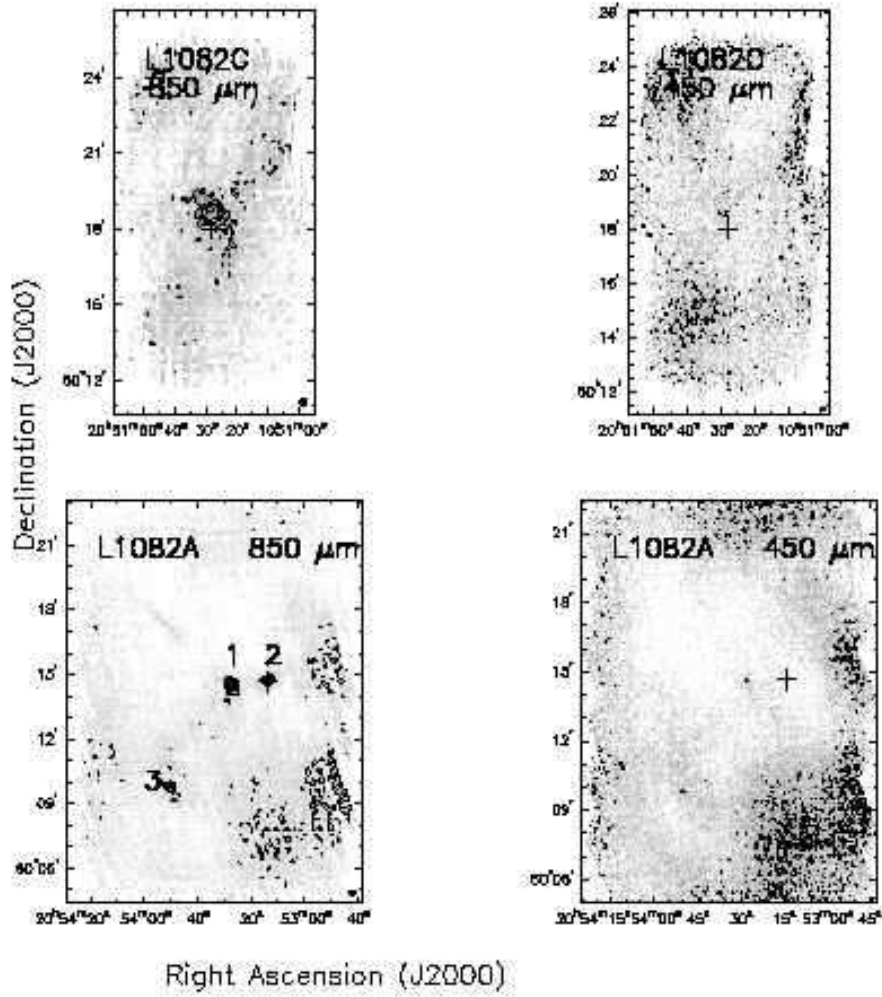


Fig. 1.— continued...

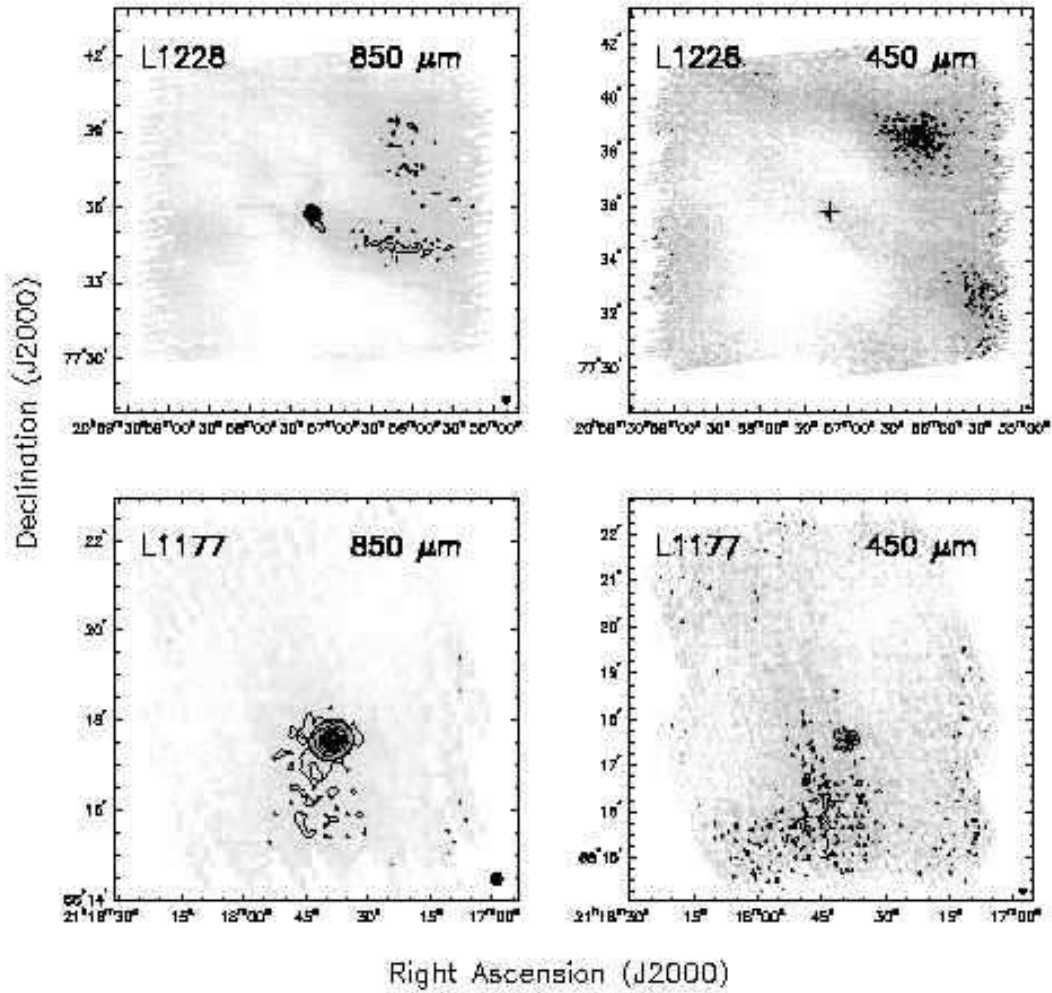


Fig. 1.— continued...

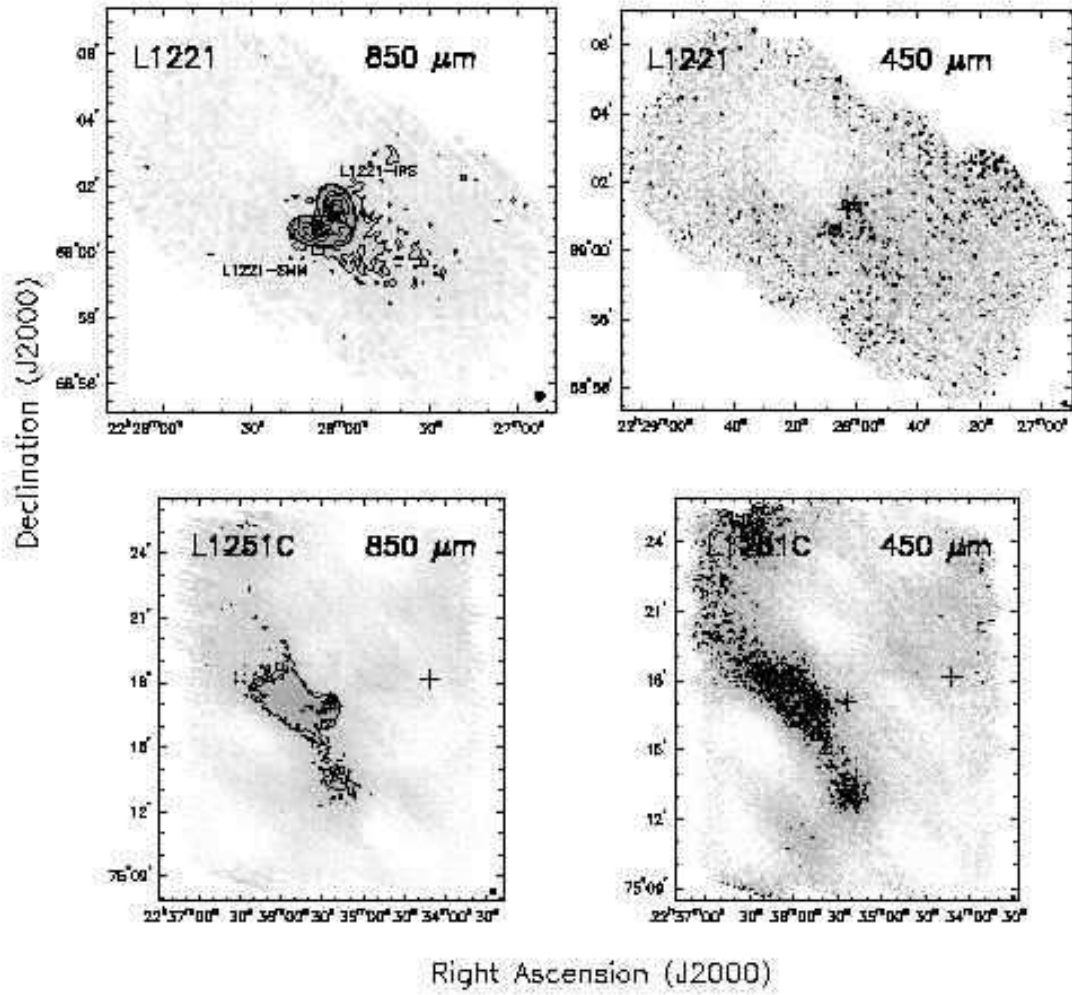


Fig. 1.— continued...

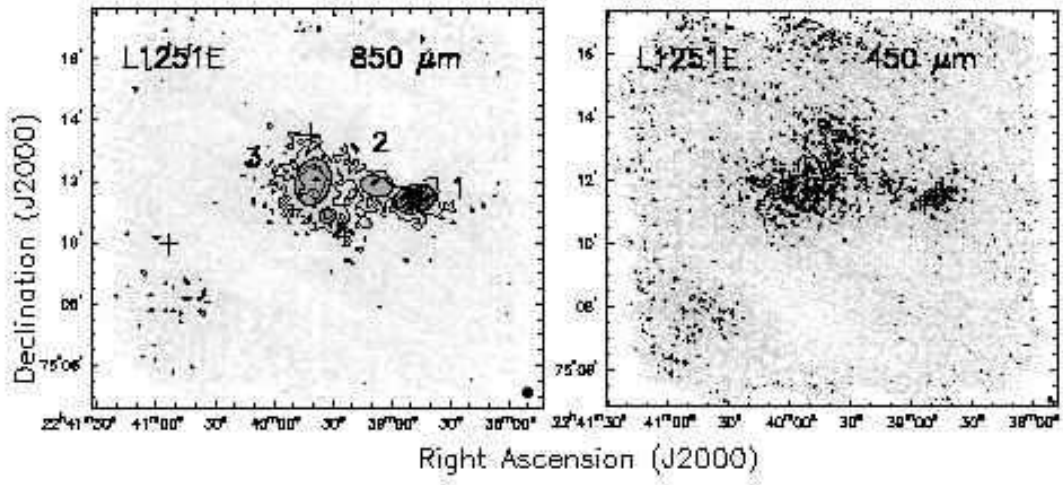


Fig. 1.— continued...



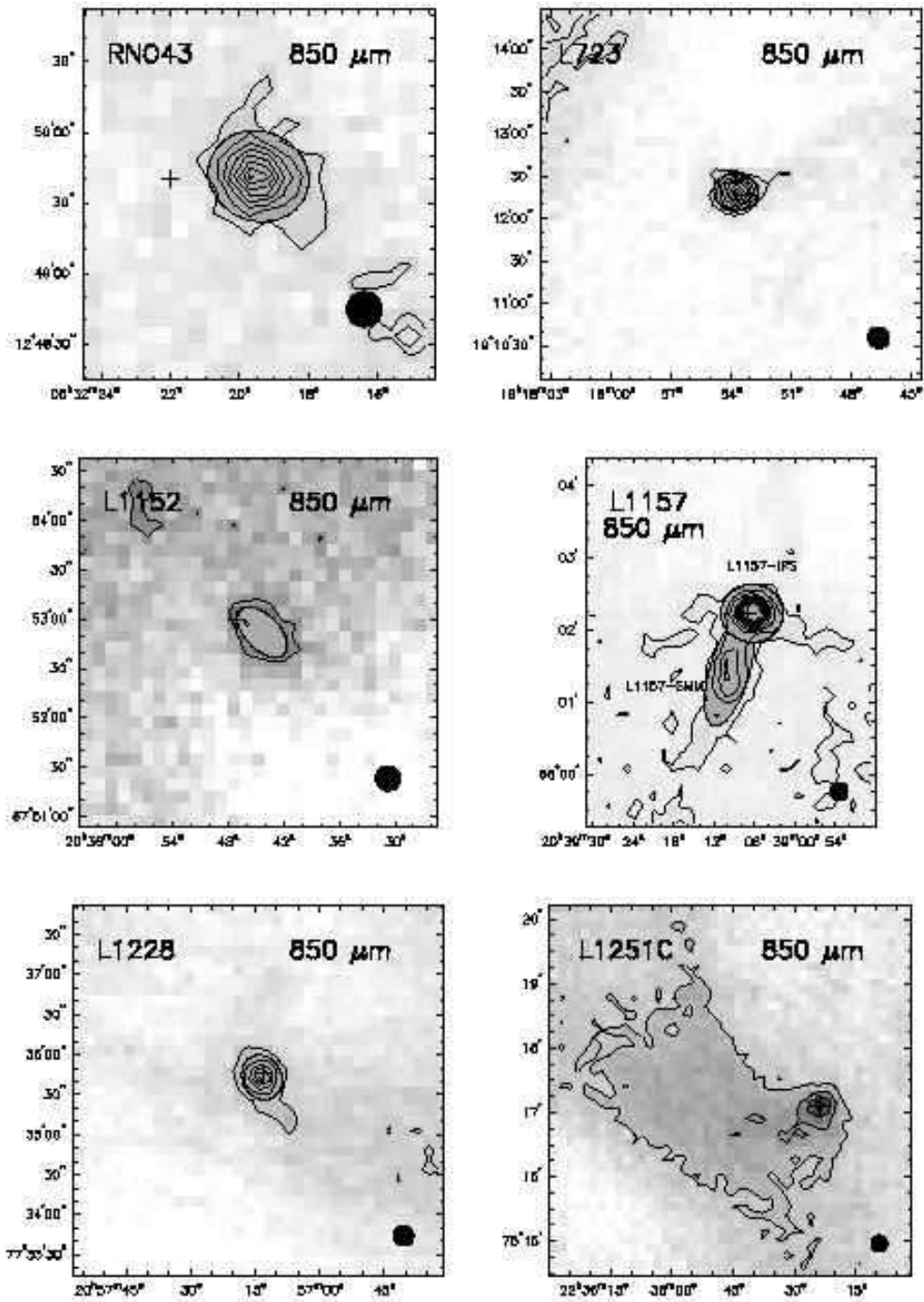


Fig. 2.— These are the central regions of those maps that cover especially large regions. The ellipses and crosses are as described for Figure 1.

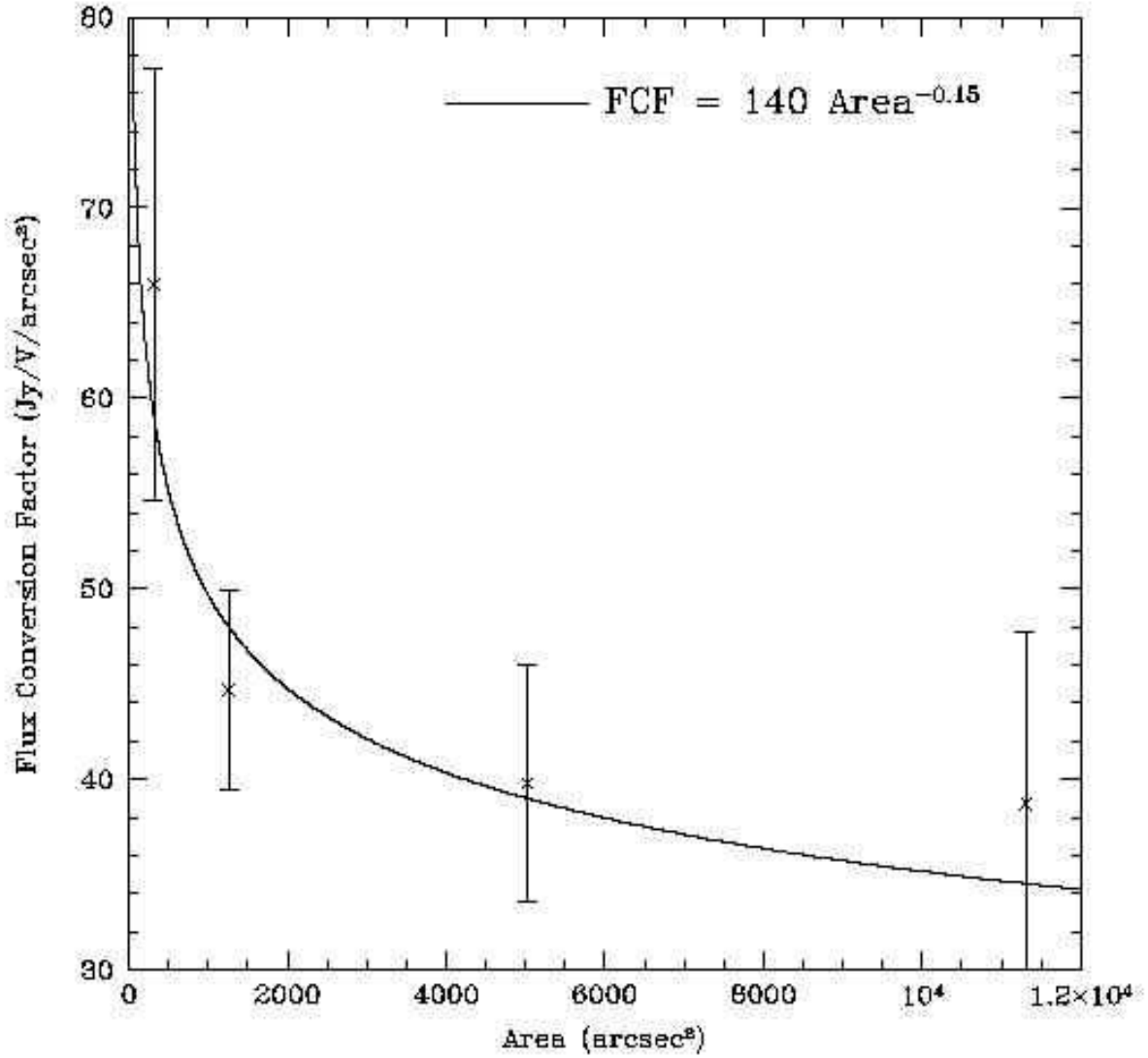


Fig. 3.— We have fitted the data for flux conversion factors (shown by the crosses) with a function in order to calculate the FCF for apertures with different area. This function ( $FCF = 140(\text{Area})^{-0.15}$ ) is used in calculating the FCFs used to determine the source fluxes

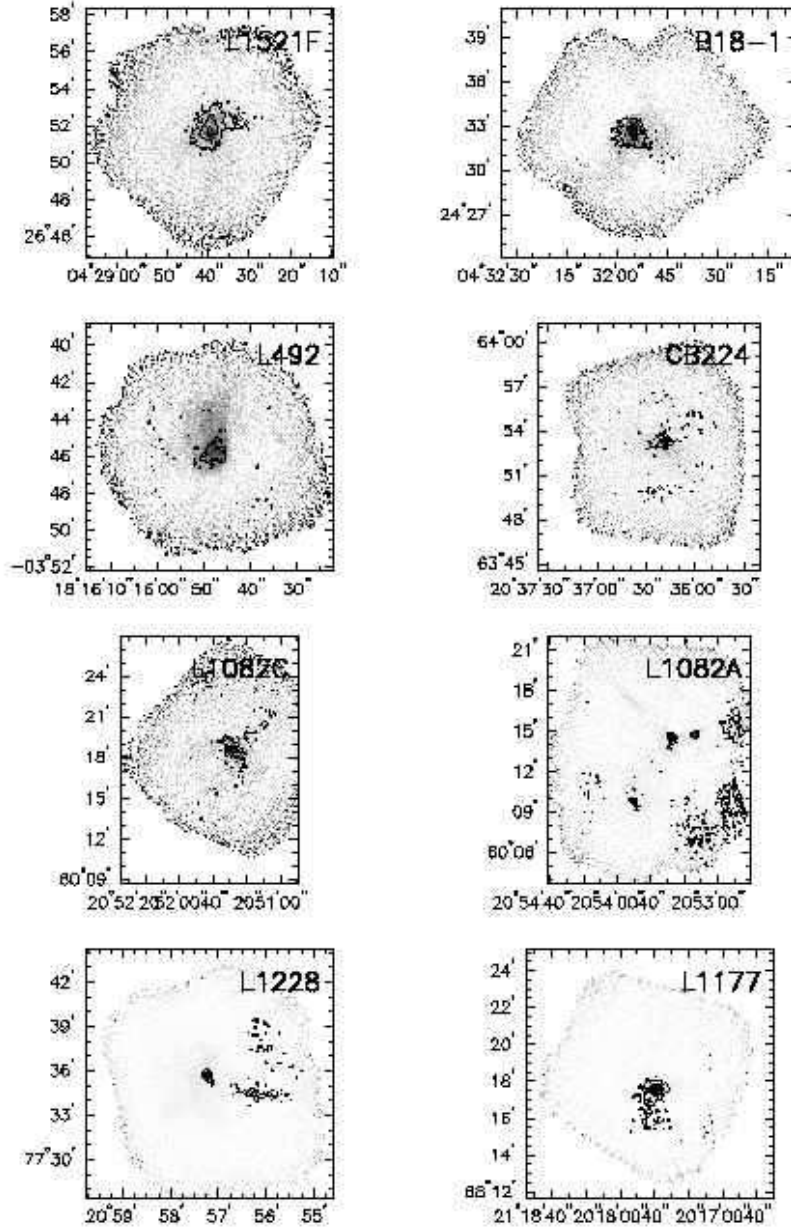


Fig. 4.— MAMBO data for cores are shown in greyscale (Kauffmann et al. 2006). The contours represent 850  $\mu\text{m}$  observations as shown in Figure 1. The SCUBA and MAMBO data show good agreement on these cores.

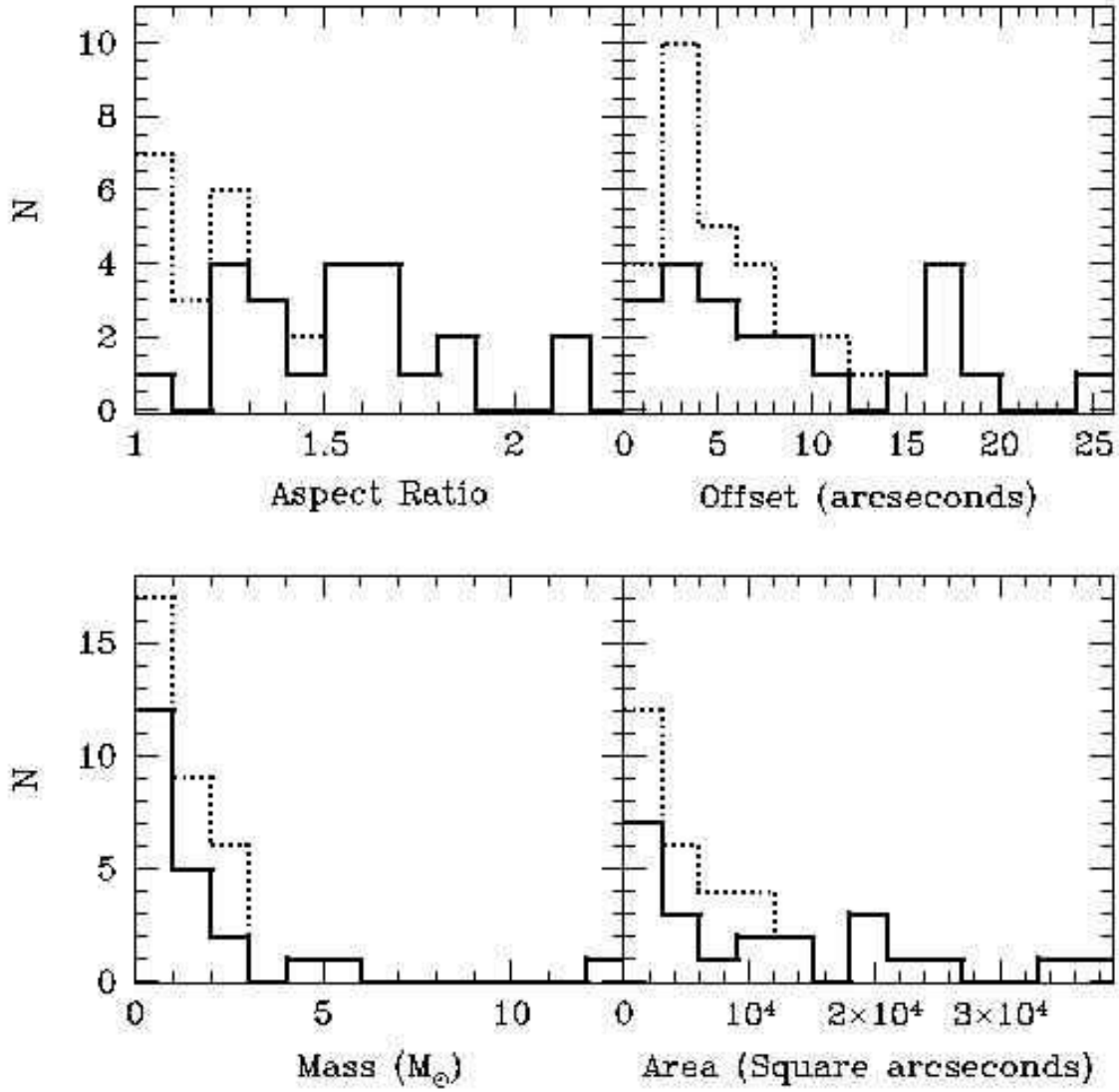


Fig. 5.— These histograms show the isothermal masses, aspect ratios, and areas as reported in Table 3. The solid line represents the data for cores observed by c2d; the dotted line shows the histogram for all cores presented in this paper. The area is calculated as  $\pi ab$ , the

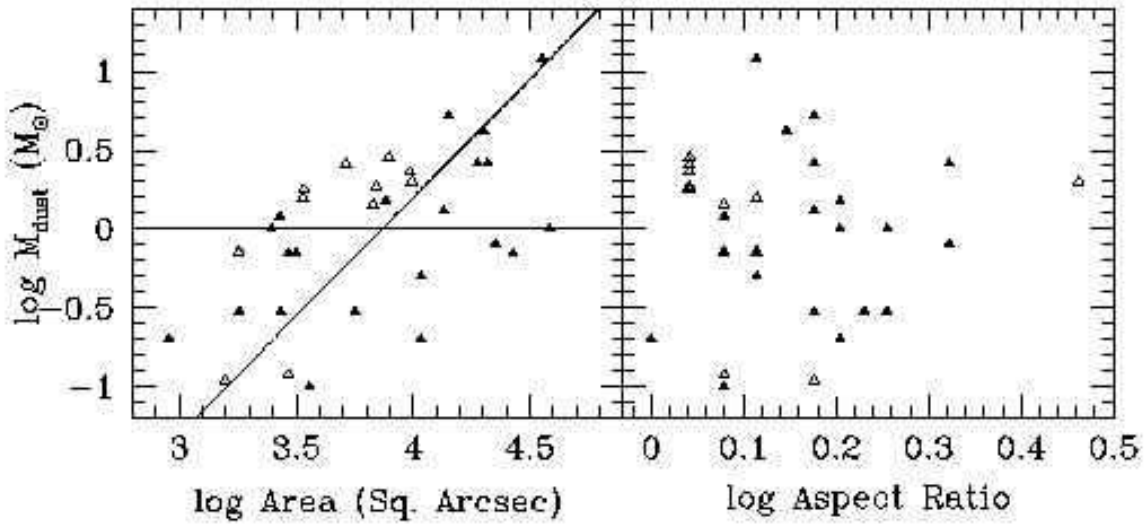


Fig. 6.— We plot the mass of each core against the size and aspect ratio as measured at the  $3\text{-}\sigma$  level. The filled triangles are for cores observed by c2d; the open triangles are for cores not observed by c2d. To calculate the dust mass, we use the flux in the elliptical aperture

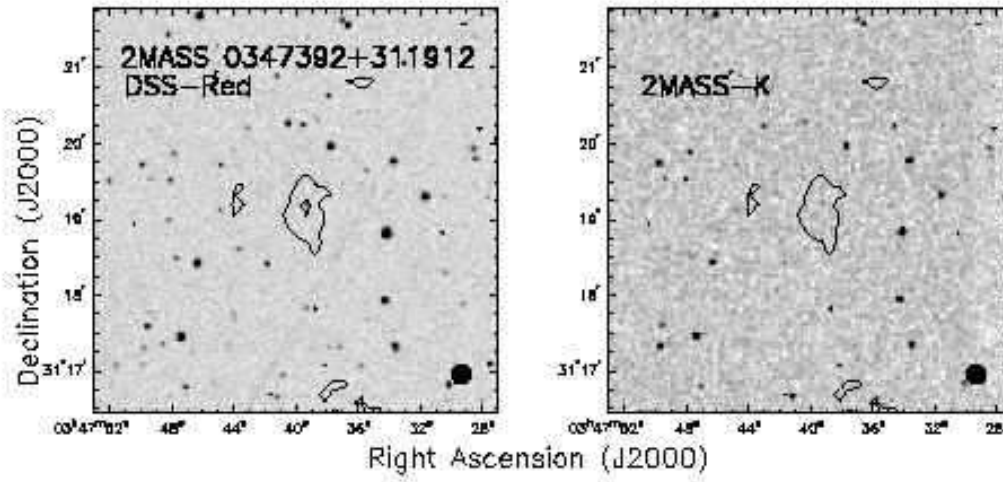


Fig. 7.— We show data for 2MASS 0347392+311912. The greyscale in the left panel is from the Digitized Sky Survey, and the right panel shows the 2MASS K-band image. The contours are from the SCUBA 850  $\mu\text{m}$  observations. Contours begin at  $2\text{-}\sigma$  and increase

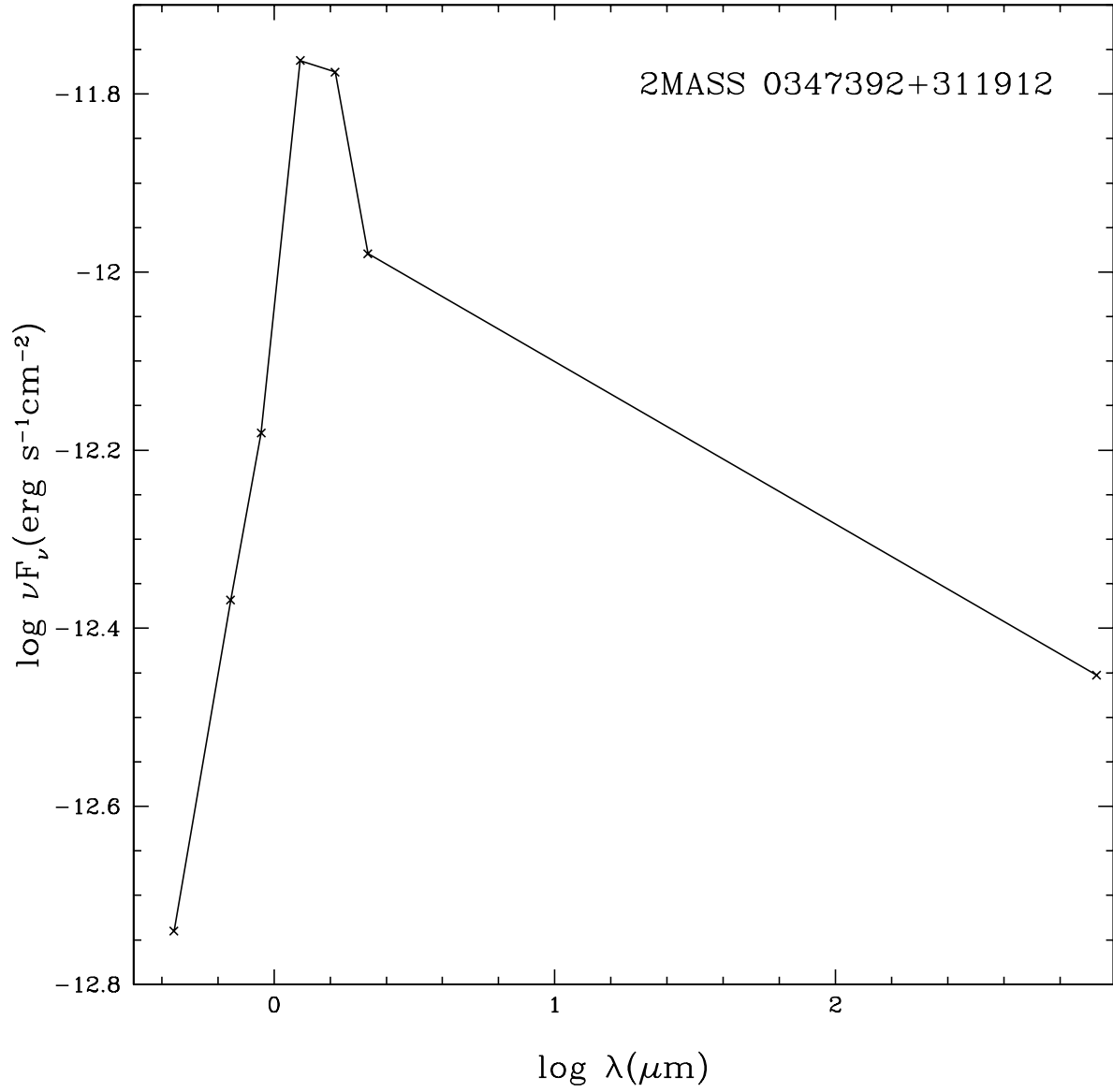


Fig. 8.— We show the SED for 2MASS 0347392+311912. The B, R, and I fluxes are from the USNO-B1.0 Catalog. J, H, and K data are from 2MASS. The 850  $\mu\text{m}$  data is from this work.

Table 1. Sources

Source Name	RA (J2000)	Dec (J2000)	Association	Dist. (pc)	Ref <sup>b</sup>	IRAS <sup>a</sup> (Y/N)	SCUBA (Y/N)	SST <sup>c</sup> (Y/N)	3- $\sigma$ (850 $\mu$ m) (mJy/beam)	3- $\sigma$ (450 $\mu$ m) (mJy/beam)	$\tau_{850}$	$\tau_{450}$
<b>PER4B</b>	03 <sup>h</sup> 29 <sup>m</sup> 17 <sup>s</sup> .9	31°27'31''	Perseus	250	1	NNY	YYY	P	220	2500	0.4	2.4
<b>PER5</b>	03 <sup>h</sup> 29 <sup>m</sup> 51 <sup>s</sup> .6	31°39'04''	Perseus	250	1	Y	Y	P	190	3900	0.44	3.0
<b>PER6</b>	03 <sup>h</sup> 30 <sup>m</sup> 14 <sup>s</sup> .9	30°23'49''	Perseus	250	1	Y	Y	P	150	6500	0.44	3.0
2MASS0347392	03 <sup>h</sup> 47 <sup>m</sup> 37 <sup>s</sup> .6	31°19'27''	Perseus	250	1	N	Y	N	110	4200	0.49	3.2
<b>IRAM04191+1522</b>	04 <sup>h</sup> 21 <sup>m</sup> 56 <sup>s</sup> .9	15°29'47''	Taurus	140	2	NY	YY	Y	120	800	0.26	1.3
<b>L1521F</b>	04 <sup>h</sup> 28 <sup>m</sup> 39 <sup>s</sup> .8	26°51'35''	Taurus	140	2	N	Y	Y	190	3100	0.29	1.6
<b>L1524-4</b>	04 <sup>h</sup> 30 <sup>m</sup> 05 <sup>s</sup> .7	24°25'16''	Taurus	140	2	N	Y	Y	200	1700	0.39	1.7
<b>B18-1</b>	04 <sup>h</sup> 31 <sup>m</sup> 57 <sup>s</sup> .7	24°32'30''	Taurus	140	2	N	Y	Y	190	5900	0.44	2.7
IRAS 04361+2547	04 <sup>h</sup> 39 <sup>m</sup> 13 <sup>s</sup> .9	25°53'21''	Taurus	140	2	Y	Y	N	180	8600	0.44	3.0
RNO43	05 <sup>h</sup> 32 <sup>m</sup> 27 <sup>s</sup> .9	12°53'11''		400	3	Y	Y	N	170	1800	0.22	1.2
<b>B35A</b>	05 <sup>h</sup> 44 <sup>m</sup> 37 <sup>s</sup> .0	09°10'13''		400	3	Y	Y	Y	220	2000	0.19	0.9
<b>L43</b>	16 <sup>h</sup> 34 <sup>m</sup> 30 <sup>s</sup> .2	-15°46'56''	Ophiuchus	125	4	YN	YY	Y	240	2700	0.27	1.5
<b>CB68</b>	16 <sup>h</sup> 57 <sup>m</sup> 20 <sup>s</sup> .5	-16°09'02''	Ophiuchus	125	4	Y	Y	Y	370	4100	0.29	1.3
<b>L492</b>	18 <sup>h</sup> 15 <sup>m</sup> 49 <sup>s</sup> .0	-03°45'30''		270	5	N	Y	Y	120	500	0.15	0.6
<b>L723</b>	19 <sup>h</sup> 17 <sup>m</sup> 53 <sup>s</sup> .2	19°12'17''		300	6	Y	Y	Y	190	1400	0.24	1.2
<b>L1152</b>	20 <sup>h</sup> 35 <sup>m</sup> 46 <sup>s</sup> .0	67°52'42''		325	7	Y	Y	Y	350	2700	0.2	0.9
CB224	20 <sup>h</sup> 36 <sup>m</sup> 20 <sup>s</sup> .3	63°52'55''		400	8	Y	Y	N	120	1000	0.19	1.0
L1157	20 <sup>h</sup> 39 <sup>m</sup> 06 <sup>s</sup> .2	68°02'42''		325	7	YN	YY	N	160	1100	0.16	0.7
L1082C	20 <sup>h</sup> 51 <sup>m</sup> 27 <sup>s</sup> .6	60°18'35''		400	8	Y	Y	N	140	2500	0.34	2.1
L1082A	20 <sup>h</sup> 53 <sup>m</sup> 34 <sup>s</sup> .0	60°13'41''		400	8	YYN	YYY	N	160	1400	0.22	1.1
<b>L1228</b>	20 <sup>h</sup> 57 <sup>m</sup> 11 <sup>s</sup> .8	77°35'48''		200	9	Y	Y	Y	350	5900	0.26	1.5
L1177 (CB230)	21 <sup>h</sup> 17 <sup>m</sup> 43 <sup>s</sup> .0	68°18'24''		288	7	Y	Y	N	180	1600	0.26	1.2
<b>L1221</b>	22 <sup>h</sup> 28 <sup>m</sup> 03 <sup>s</sup> .0	69°01'12''		250	10	YN	YY	Y	160	2400	0.31	1.8
<b>L1251C</b>	22 <sup>h</sup> 35 <sup>m</sup> 24 <sup>s</sup> .0	75°17'09''		300	11	Y	Y	Y	330	4800	0.26	1.5
<b>L1251E</b>	22 <sup>h</sup> 38 <sup>m</sup> 20 <sup>s</sup> .7	75°11'03''		300	11	YNYN	YYYY	Y	260	5300	0.29	1.6
<b>PER7A</b>	03 <sup>h</sup> 32 <sup>m</sup> 26 <sup>s</sup> .6	30°59'57''	Perseus	250	1	Y	N	P	200	1800	0.37	2.2
<b>PER7B</b>	03 <sup>h</sup> 33 <sup>m</sup> 15 <sup>s</sup> .3	30°59'54''	Perseus	250	1	N	N	P	140	1500	0.35	2.1
<b>L1521B-2</b>	04 <sup>h</sup> 23 <sup>m</sup> 37 <sup>s</sup> .0	26°40'06''	Taurus	140	2	N	N	Y	190	2300	0.4	2.4
<b>L1521-2</b>	04 <sup>h</sup> 29 <sup>m</sup> 31 <sup>s</sup> .8	26°59'59''	Taurus	140	2	N	N	Y	260	1600	0.39	1.7
<b>B18-5</b>	04 <sup>h</sup> 35 <sup>m</sup> 53 <sup>s</sup> .0	24°09'32''	Taurus	140	2	N	N	Y	180	9500	0.51	3.8
<b>TMC1-2</b>	04 <sup>h</sup> 41 <sup>m</sup> 10 <sup>s</sup> .0	25°49'28''	Taurus	140	2	Y	N	Y	320	4800	0.55	2.7
<b>TMC1-1</b>	04 <sup>h</sup> 41 <sup>m</sup> 44 <sup>s</sup> .0	25°42'22''	Taurus	140	2	N	N	Y	190	24900	0.38	2.9
CB28	05 <sup>h</sup> 06 <sup>m</sup> 16 <sup>s</sup> .0	-03°56'29''		450	12	Y	N	N	350	6400	0.25	1.7
DCld 253.6+02.9	08 <sup>h</sup> 28 <sup>m</sup> 44 <sup>s</sup> .0	-33°45'12''		450	13	Y	N	N	330	7400	0.22	1.2



Table 1—Continued

Source Name	RA (J2000)	Dec (J2000)	Association	Dist. (pc)	Ref <sup>b</sup>	IRAS <sup>a</sup> (Y/N)	SCUBA (Y/N)	SST <sup>c</sup> (Y/N)	3- $\sigma$ (850 $\mu$ m) (mJy/beam)	3- $\sigma$ (450 $\mu$ m) (mJy/beam)	$\tau_{850}$	$\tau_{450}$
<b>L1772</b>	17 <sup>h</sup> 19 <sup>m</sup> 32 <sup>s</sup> .7	-26°44′4″0	Ophiuchus	125	4	N	N	Y	260	2900	0.26	1.5
L55	17 <sup>h</sup> 22 <sup>m</sup> 58 <sup>s</sup> .0	-23°57′18″	Ophiuchus	125	4	N	N	N	280	3100	0.25	1.2
<b>B72</b>	17 <sup>h</sup> 23 <sup>m</sup> 46 <sup>s</sup> .3	-23°41′20″	Ophiuchus	125	4	N	N	Y	340	4100	0.32	1.9
<b>L1155C</b>	20 <sup>h</sup> 43 <sup>m</sup> 06 <sup>s</sup> .0	67°49′56″		325	7	Y	N	Y	210	1700	0.21	1.0

<sup>a</sup>We search a 1′ radius for detections by IRAS. The IRAS sources must meet the criteria presented by Lee & Myers (1999). More than one symbol implies that more than one submillimeter core was found.

<sup>b</sup>(1)Enoch et al. (2006),(2)Elias (1978),(3)Murdin & Penston (1977),(4)de Geus et al. (1989),(5)Straizys et al. (2003), (6)Goldsmith et al. (1984),(7)Straizys et al. (1992),(8)Dobashi et al. (1994),(9)Kun (1998),(10)Yonekura et al. (1997), (11)Kun & Prusti (1993),(12)Ogura & Sugitani (1998),(13)Woermann et al. (2001)

<sup>c</sup>A Y means that the core was observed by Spitzer (SST) as part of the c2d cores program, a N means that it was in the original cores program, but was cut; and a P means that it was observed as part of the Perseus cloud map.

Table 2. Calibrators

Date	Calibrator	$\tau_{850}$	$\tau_{450}$	$C_{20}^{850a}$	$C_{40}^{850}$	$C_{80}^{850}$	$C_{120}^{850}$	$C_{20}^{450}$	$C_{40}^{450}$	$C_{80}^{450}$	$C_{120}^{450}$	FWHM <sup>c</sup> (")
11 Jan 2002	CRL618	0.26	1.31	79.0	41.4	31.5	24.6	38.3	22.2	10.5	6.0	15.3
11 Jan 2002	Uranus	0.20	0.96	62.0	44.0	41.5	42.0	35.1	29.5	28.7	33.8	15.6
15 Jan 2002	CRL618	0.40	2.37	61.8	41.5	31.9	25.0	23.6	12.6	5.6	3.1	15.5
15 Jan 2002	Mars	0.35	2.14	62.8	47.3	43.6	42.9	34.2	25.9	21.5	19.8	15.0
15 Jan 2002	Uranus	0.37	2.17	68.1	47.7	45.3	46.6	31.9	32.0	119.2	-21.5	15.9
17 Jan 2002	CRL618	0.51	3.84	57.5	43.8	41.9	43.3	12.4	10.7	10.0	9.8	15.5
17 Jan 2002	CRL618	0.44	3.03	76.9	47.8	43.6	42.5	24.4	15.9	7.8	5.5	15.8
17 Jan 2002	Mars	0.52	3.24	80.6	49.6	45.1	43.9	29.5	21.8	17.1	15.3	15.5
18 Jan 2002	CRL618	0.60	4.28	76.6	38.9	27.1	19.8	5.8	2.3	0.9	0.4	16.6
18 Jan 2002	CRL618	0.60	4.28	67.0	48.0	47.9	55.5	16.6	17.7	-8.4	-2.6	15.4
18 Jan 2002	Mars	0.55	2.69	72.0	49.3	43.1	41.0	66.3	46.5	36.0	31.4	15.5
29 Oct 2002	Jupiter <sup>b</sup>	0.25	1.34	155.8	68.3	50.4	48.8	198.6	68.7	49.6	47.0	...
29 Oct 2002	Uranus	0.28	1.50	71.2	55.1	52.6	53.5	74.4	64.8	89.2	917.1	15.7
23 Mar 2003	IRC10216 <sup>b</sup>	0.18	0.97	54.6	30.9	25.4	26.2	...	...	...	...	...
23 Mar 2003	IRC10216	0.17	0.88	52.6	29.4	24.0	24.6	...	...	...	...	...
25 Mar 2003	IRC10216	0.33	1.94	48.5	25.6	16.6	12.8	...	...	...	...	...
26 Mar 2003	IRC10216	0.35	2.11	50.9	28.8	26.2	27.8	...	...	...	...	...
26 Mar 2003	Mars	0.25	1.45	61.7	42.3	39.0	38.7	54.6	40.9	36.4	36.5	15.5
27 Mar 2003	IRC10216	0.30	1.57	54.0	29.8	23.6	22.5	...	...	...	...	...
28 Mar 2003	IRC10216	0.20	0.87	45.1	24.6	17.7	15.0	...	...	...	...	...
20 May 2003	Uranus	0.19	0.96	48.4	37.8	35.4	35.4	35.7	28.6	26.0	26.1	14.4
20 May 2003	Uranus	0.16	0.72	56.2	39.8	37.8	37.5	50.2	38.7	33.8	34.3	15.4
22 May 2003	Uranus	0.22	1.07	56.8	38.9	34.6	34.1	41.7	28.4	24.7	23.8	16.0
23 May 2003	Uranus	0.24	1.22	52.4	40.0	37.3	36.8	51.0	41.6	37.1	35.6	15.3
27 May 2003	Uranus	0.37	2.55	53.0	40.4	37.7	37.1	25.2	20.0	17.6	17.3	15.1
Average Values (Standard Deviation)				65(10)	44(5)	40(6)	39(9)	36(18)	28(15)	28(31)	...	15''5(0''5)

<sup>a</sup>The calibration factor, in Jy/V, for a 40'' aperture. Also, we show the 80'' and 120'' calibration factors.

<sup>b</sup>We do not include Jupiter or IRC10216 in the average calibration factor.

<sup>c</sup>We give the FWHM of the beam at 850  $\mu\text{m}$ . We deconvolve the measured beam size for the planet diameter; Uranus and Mars have semi-diameters of 1''72 and 3''67, respectively

Table 3. Source Properties at  $3\text{-}\sigma$  Contours

Source	RA J2000	Dec J2000	Major Axis (")	Minor Axis (")	Aspect Ratio	$S_\nu$ <sup>a</sup> (Jy)	$M_{core}$ <sup>b</sup> ( $M_\odot$ )
<b>PER4-B</b>	03 <sup>h</sup> 29 <sup>m</sup> 17 <sup>s</sup> .2	31°27'53"	22	13	1.6	0.3(0.1)	0.2(0.1)
<b>PER4-C</b>	03 <sup>h</sup> 29 <sup>m</sup> 18 <sup>s</sup> .2	31°25'14"	29	20	1.5	0.5(0.2)	0.3(0.1)
<b>PER4-A</b>	03 <sup>h</sup> 29 <sup>m</sup> 25 <sup>s</sup> .3	31°28'20"	17	17	1	0.3(0.1)	0.2(0.1)
<b>PER5</b>	03 <sup>h</sup> 29 <sup>m</sup> 51 <sup>s</sup> .8	31°39'11"	80	54	1.5	2.4(0.7)	1.3(0.4)
2MASS0347392	03 <sup>h</sup> 47 <sup>m</sup> 39 <sup>s</sup> .4	31°19'08"	27	18	1.5	0.2(0.1)	0.1(0.03)
<b>IRAM 04191+1522</b>	04 <sup>h</sup> 21 <sup>m</sup> 56 <sup>s</sup> .8	15°29'51"	75	46	1.6	1.4(0.4)	0.2(0.1)
<b>IRAS 04191+1523</b>	04 <sup>h</sup> 22 <sup>m</sup> 00 <sup>s</sup> .6	15°30'26"	38	30	1.2	0.6(0.2)	0.1(0.03)
<b>L1521F</b>	04 <sup>h</sup> 28 <sup>m</sup> 39 <sup>s</sup> .7	26°51'51"	142	87	1.6	5.9(1.8)	1.0(0.3)
<b>L1524-4</b>	04 <sup>h</sup> 30 <sup>m</sup> 03 <sup>s</sup> .0	24°26'39"	9	9	1	0.1(0.03)	0.02(0.01)
<b>B18-1</b>	04 <sup>h</sup> 31 <sup>m</sup> 55 <sup>s</sup> .8	24°32'35"	104	82	1.3	4.1(1.2)	0.7(0.2)
IRAS 04361+2547	04 <sup>h</sup> 39 <sup>m</sup> 14 <sup>s</sup> .0	25°53'23"	34	27	1.2	0.7(0.2)	0.1(0.04)
RNO43	05 <sup>h</sup> 32 <sup>m</sup> 19 <sup>s</sup> .4	12°49'41"	43	38	1.1	1.8(0.5)	2.6(0.8)
<b>B35A</b>	05 <sup>h</sup> 44 <sup>m</sup> 31 <sup>s</sup> .1	09°09'04"	119	95	1.3	8.3(2.5)	12.0(3.6)
<b>L43-IRS</b>	16 <sup>h</sup> 34 <sup>m</sup> 30 <sup>s</sup> .1	-15°46'59"	55	33	1.7	1.8(0.5)	0.3(0.1)
<b>L43-SMM</b>	16 <sup>h</sup> 34 <sup>m</sup> 35 <sup>s</sup> .8	-15°47'07"	123	58	2.1	5.7(1.7)	0.8(0.2)
<b>CB68</b>	16 <sup>h</sup> 57 <sup>m</sup> 19 <sup>s</sup> .6	-16°09'20"	68	51	1.3	3.9(1.2)	0.5(0.2)
<b>L492</b>	18 <sup>h</sup> 15 <sup>m</sup> 47 <sup>s</sup> .8	-03°45'51"	39	22	1.8	0.4(0.1)	0.3(0.1)
<b>L723</b>	19 <sup>h</sup> 17 <sup>m</sup> 53 <sup>s</sup> .7	19°12'19"	32	27	1.2	1.5(0.5)	1.2(0.4)
<b>L1152</b>	20 <sup>h</sup> 35 <sup>m</sup> 44 <sup>s</sup> .3	67°52'52"	38	21	1.8	1(0.3)	1.0(0.3)
CB224	20 <sup>h</sup> 36 <sup>m</sup> 18 <sup>s</sup> .5	63°53'16"	51	42	1.2	1(0.3)	1.4(0.4)
L1157-IRS	20 <sup>h</sup> 39 <sup>m</sup> 06 <sup>s</sup> .3	68°02'14"	52	48	1.1	3(0.9)	2.9(0.9)
L1157-SMM	20 <sup>h</sup> 39 <sup>m</sup> 09 <sup>s</sup> .7	68°01'26"	95	33	2.9	2.1(0.6)	2.0(0.6)
L1082C	20 <sup>h</sup> 51 <sup>m</sup> 28 <sup>s</sup> .2	60°18'38"	50	45	1.1	1.3(0.4)	1.9(0.6)
L1082A-2	20 <sup>h</sup> 53 <sup>m</sup> 13 <sup>s</sup> .7	60°14'42"	26	22	1.2	0.5(0.2)	0.7(0.3)
L1082A-1	20 <sup>h</sup> 53 <sup>m</sup> 27 <sup>s</sup> .6	60°14'34"	38	28	1.3	1.1(0.3)	1.6(0.6)
L1082A-3	20 <sup>h</sup> 53 <sup>m</sup> 50 <sup>s</sup> .2	60°09'47"	27	21	1.3	0.5(0.2)	0.7(0.3)
<b>L1228</b>	20 <sup>h</sup> 57 <sup>m</sup> 13 <sup>s</sup> .4	77°35'43"	34	29	1.2	2(0.6)	0.7(0.2)
L1177	21 <sup>h</sup> 17 <sup>m</sup> 38 <sup>s</sup> .8	68°17'33"	59	52	1.1	3.1(0.9)	2.3(0.7)
L1251C <sup>c</sup>	22 <sup>h</sup> 35 <sup>m</sup> 24 <sup>s</sup> .6	75°17'04"	35	31	1.1	2.2(0.7)	1.8(0.5)
<b>L1221-IRS</b>	22 <sup>h</sup> 28 <sup>m</sup> 01 <sup>s</sup> .4	69°01'18"	95	63	1.5	4.7(1.4)	2.6(0.8)

Table 3—Continued

Source	RA J2000	Dec J2000	Major Axis (")	Minor Axis (")	Aspect Ratio	$S_\nu$ <sup>a</sup> (Jy)	$M_{core}$ <sup>b</sup> ( $M_\odot$ )
<b>L1221-SMM</b>	22 <sup>h</sup> 28 <sup>m</sup> 06 <sup>s</sup> .9	69°00′38″	117	57	2.1	4.7(1.4)	2.6(0.8)
<b>L1251E-1</b>	22 <sup>h</sup> 38 <sup>m</sup> 48 <sup>s</sup> .1	75°11′26″	83	55	1.5	6.4(1.9)	5.2(1.6)
<b>L1251E-2</b>	22 <sup>h</sup> 39 <sup>m</sup> 07 <sup>s</sup> .7	75°11′51″	62	39	1.6	1.9(0.6)	1.5(0.5)
<b>L1251E-4</b>	22 <sup>h</sup> 39 <sup>m</sup> 32 <sup>s</sup> .3	75°10′53″	33	28	1.2	0.9(0.3)	0.7(0.2)
<b>L1251E-3</b>	22 <sup>h</sup> 39 <sup>m</sup> 40 <sup>s</sup> .0	75°11′59″	93	68	1.4	5.2(1.6)	4.2(1.3)

<sup>a</sup>We give the 850  $\mu\text{m}$  flux calculated for the elliptical aperture described in this table.

<sup>b</sup>The mass of the core is derived from the 850  $\mu\text{m}$  flux assuming an isothermal temperature of 15 K.

<sup>c</sup>As discussed in the text, the properties of L1251C were calculated with the analysis threshold set to  $5\text{-}\sigma$ .

Table 4. Source Fluxes

Source Name	$S_{20}^{850\text{a}}$	$S_{40}^{850}$	$S_{80}^{850}$	$S_{120}^{850}$	$S_{20}^{450}$	$S_{40}^{450}$
<b>PER4-B</b>	0.5(0.09)	0.7(0.1)	0.9(0.2)	0.6(0.3)	2.0(1.1)	2.8(1.6)
<b>PER4-C</b>	0.4(0.08)	0.9(0.1)	1.4(0.3)	2.0(0.5)	2.1(1.1)	4.4(2.4)
<b>PER4-A</b>	0.3(0.05)	0.6(0.1)	0.9(0.2)	0.9(0.3)	3.3(1.7)	7.7(4.2)
<b>PER5</b>	0.8(0.14)	1.3(0.2)	3.0(0.5)	4.9(1.2)	5.6(2.9)	11.9(6.4)
2MASS0347392	0.2(0.04)	0.5(0.1)	0.9(0.2)	1.1(0.3)	...	...
<b>IRAM 04191+1522</b>	0.5(0.09)	0.9(0.1)	1.8(0.3)	2.8(0.7)	1.6(0.8)	1.1(0.7)
<b>IRAS 04191+1523</b>	0.4(0.07)	0.6(0.1)	1.2(0.2)	1.9(0.5)	1.4(0.7)	1.4(0.8)
<b>L1521F</b>	0.6(0.10)	1.5(0.2)	4.2(0.7)	6.8(1.6)	4.6(2.4)	13.3(7.2)
<b>L1524-4</b>	0.3(0.05)	0.6(0.1)	1.9(0.3)	3.8(0.9)	2.0(1.0)	5.6(3.0)
<b>B18-1</b>	0.3(0.04)	1.1(0.1)	3.4(0.6)	6.1(1.5)	9.1(4.6)	22.8(12.3)
IRAS 04361+2547	0.5(0.08)	0.8(0.1)	1.5(0.3)	1.9(0.5)	... <sup>b</sup>	...
RNO43	1.2(0.2)	1.7(0.3)	2.3(0.5)	2.7(0.7)	8.8(4.4)	13.8(7.5)
<b>B35A</b>	0.8(0.13)	2.6(0.3)	6.7(1.1)	10.0(2.4)	3.5(1.7)	12.2(6.6)
<b>L43-IRS</b>	0.6(0.10)	1.4(0.2)	2.9(0.5)	4.8(1.2)	5.9(3.0)	15.0(8.1)
<b>L43-SMM</b>	0.7(0.11)	2.0(0.2)	5.2(0.8)	8.2(2.0)	...	...
<b>CB68</b>	1.1(0.17)	2.3(0.3)	5.5(0.9)	9.4(2.3)	10.8(5.4)	27.8(14.9)
<b>L492</b>	0.2(0.03)	0.5(0.1)	1.4(0.2)	2.1(0.5)	0.7(0.3)	1.7(0.9)
<b>L723</b>	1.4(0.26)	1.4(0.3)	1.2(0.4)	0.3(0.4)	4.0(2.1)	0.7(0.9)
<b>L1152</b>	0.5(0.08)	1.2(0.2)	2.2(0.4)	2.9(0.7)	2.9(1.4)	8.3(4.4)
CB224	0.4(0.07)	0.8(0.1)	1.5(0.3)	1.9(0.5)	2.3(1.2)	2.8(1.6)
L1157-SMM	0.7(0.11)	1.2(0.2)	2.5(0.4)	5.7(1.4)	...	...
L1157-IRS	2.2(0.39)	2.5(0.5)	3.7(0.8)	5.0(1.3)	9.7(4.9)	13.2(7.2)
L1082C	0.3(0.05)	1.0(0.1)	2.2(0.4)	3.4(0.8)	1.9(1.0)	4.8(2.6)
L1082A-2	0.4(0.07)	0.6(0.1)	0.8(0.2)	0.5(0.2)	...	...
L1082A-1	0.8(0.15)	1.1(0.2)	1.5(0.3)	1.7(0.5)	1.1(0.6)	0.02(0.4)
L1082A-3	0.5(0.08)	0.6(0.1)	1.1(0.2)	1.7(0.4)	1.7(0.9)	1.8(1.0)
<b>L1228</b>	1.2(0.20)	2.0(0.3)	3.5(0.7)	4.5(1.2)	3.6(2.1)	1.1(1.4)
L1177	1.6(0.29)	2.4(0.4)	3.9(0.7)	5.3(1.3)	6.3(3.2)	10.7(5.8)
L1251C	0.9(0.2)	2.3(0.3)	5.2(0.9)	8.7(2.1)	8.9(4.5)	16.4(8.9)
<b>L1221-IRS</b>	1.0(0.16)	2.0(0.2)	4.9(0.8)	8.1(2.0)	4.9(2.5)	10.4(5.6)
<b>L1221-SMM</b>	1.2(0.19)	2.0(0.3)	4.5(0.8)	7.9(1.9)	6.5(3.3)	11.3(6.1)
<b>L1251E-1</b>	2.0(0.33)	4.0(0.5)	7.0(1.3)	9.5(2.3)	24.1(12.1)	49.5(26.6)
<b>L1251E-2</b>	0.5(0.08)	1.4(0.2)	3.5(0.6)	5.9(1.4)	...	...
<b>L1251E-4</b>	0.6(0.10)	1.2(0.2)	3.3(0.5)	6.6(1.6)	...	...
<b>L1251E-3</b>	0.5(0.09)	1.9(0.2)	5.2(0.8)	9.4(2.2)	...	...

<sup>a</sup>The flux, in Jy, for a 20'' aperture. The remaining columns are fluxes in 40'', 80'', and 120'' apertures. We also give the 450  $\mu\text{m}$  fluxes as measured in 20'' and 40'' apertures.

<sup>b</sup>We require, at least, a 2- $\sigma$  detection to report the flux measurement; several cores did not satisfy this requirement in the 450  $\mu\text{m}$  data.